The conductivity properties of protons in ice and mechanism of magnetization of liquid water

X.F. Pang[a]

Institute of Life Science and Technology, University of Electronic Science and Technology of China, Chengdu 610054, P.R. China
and
International Centre for Materials Physics, Chinese Academy of Sciences, Shenyang 110015, P.R. China

Abstract. From a study of electrical conductivity of protons in the hydrogen-bonded chains in ice we confirm that the magnetization of liquid water is caused by proton transfer in closed hydrogen-bonded chains occurring as a first order phase transition, through which the ice becomes liquid water. We first study the conductive properties of proton transfer along molecular chains in ice crystals in our model. Ice is a typical hydrogen-bonded molecular system, in which the interaction of localized fluctuation of hydrogen ions (H^+) with deformation of a structure of hydroxyl group (OH) results in soliton motion of the protons along the molecular chains via ionic and bonded defects. We explain further the quantum conductive properties of proton transfer and determine its mobility and conductivity under constant electric-field using a new theory of proton transfer, which agree with experimental values. From features of first order phase-transition for ice, and some experimental data of pure and magnetized water we confirm further that there are not only free water molecules, but also many linear and closed hydrogen-bonded chains consisting of many polarized water-molecules in the liquid water. Thus a ring proton-current, which resembles to a "molecular current" or a "small magnet" in solids, can occur in the closed hydrogen-bond chains under action of an externally applied magnetic field. Then the water molecules in the closed chains can be orderly arrayed due to the magnetic interaction among these ring proton currents and the externally applied magnetic field. This is just the magnetized effect of the water. In such a case the optical and electronic properties of the water, including the dielectric constant, magnetoconductivity, refraction index, Raman and Infrared absorption spectra, are changed. We determine experimentally the properties of the magnetized water which agree with the theoretical results of our model. However, the magnetized effect of water is, in general, very small, and vanishes at temperatures above 100 °C.

PACS. 66.30.Lw Diffusion of other defects – 03.65.Ge Solutions of wave equations: bound states – 61.20.Gy Theory and models of liquid structure

1 Introduction

Water is a very familiar form of matter because it is closely related with the growth and life of human beings, animals and plants. We can say that there is no life without water in the world. However, the properties of water are not known clearly as yet, although it has been studied for several hundreds of years. Magnetization of liquid water is a typical example. At present, we know experimentally that liquid water can be magnetized, i.e., when the water is exposed to magnetic fields, its optical, electromagnetic, thermodynamic and mechanical properties, including its density, surface tension force, viscous coefficient, boiling point, melting point, dielectric constant, conductivity, refractive index, spectra of ultraviolet and infrared and laser-Raman, all change as compared with water without magnetization [1–10]. These changes of properties are just an indication of magnetization of liquid water. Thus magnetized water has been

extensively utilized in industry, agriculture and medicine, for example, it is helpful to aid digestion of food and eliminate dirt in Industrial boilers, and so on. However, the mechanism of the magnetization has not been previously explained, although many models, for instance, Ke LaXin's resonant model [4] and models of the destruction of hydrogen bonds [5,6] and physical-chemistry reaction of water molecules with ions [7–10], were proposed. In the resonant model, Ke LaXin proposes [4] that the magnetization of water is caused by a resonant effect among vibrations of the components including the water molecules and hydrates, chelate and impurities under an externally applied magnetic field with appropriate frequency, in which the hydrogen bonds distort, so that the structure and features of water molecules change. Jiang Yijian, et al. [7–10] propose that the molecules form hydration ions with some ions in the water. The ionic hydrations which occur change the distribution, polarization and dynamic features of water molecules. The externally applied magnetic field destroys the structure
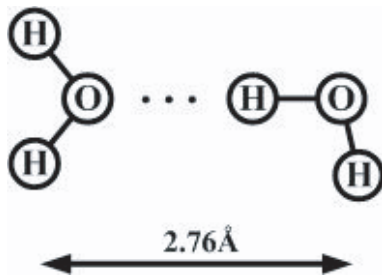
[a] e-mail: pangxf@mail.sc.cninfo.net

Fig. 1. Water dimer (H$_2$O)$_2$.

and distribution of the ionic hydrations via a Lorenz force. Their re-arrangements cause magnetization of the water to occur. They think that some hydrogen bonds were destroyed in this process. These models are only qualitative, and cannot clearly theoretically explain the magnetization of water and its properties. New ideas from nonlinear dynamics have provided a possibility to find a solution to this problem. In this paper we propose a nonlinear theory to explain the magnetization mechanism and determine its properties. The mechanism and theoretical model is based on the theory of proton conductivity in hydrogen-bonded systems consisting of the water molecules in an ice crystal, and properties of pure and magnetized water, in other words, it is a generalization of the theory of proton conductivity in ice because we know that the liquid water comes from ice at the melting point 0 °C, through a first-order phase transition. In order to shed light on the physical mechanism of the magnetized water we have to study first the theory of proton transfer in ice in Section 2 and calculate the protonic mobility and conductivity in the system in Section 3. Finally we propose the mechanism of magnetization of the liquid water from states and distribution of the water molecules in this system, give and explain the features of magnetized water by this theory in Section 4.

2 The theory of quantum proton transfer in ice crystal

As is known, water molecules consist of two hydrogen atoms and one oxygen atom with high electronegativity. When a great number of water molecules construct ice below 0 °C, the water molecules are polarized, each water molecule has a large electrical dipolar moment about 1.84 Debye (here an O-H bond is about 1.51 Debye) [11–22]. This is a most generic and distinct feature of water molecules which can be shown by a few experiments. Hydrogen bonds between neighboring molecules occur in the ice, i.e., the hydrogen atom associated with one oxygen atom in a covalent bond in one molecule incorporates with another in another molecule in a weak long-bond. In this way relatively stable dimers, for example, dimer (H$_2$O)$_2$ shown in Figure 1, and other polymeric complexes can be obtained. On average each molecule has four neighbors in ice. The composition and structure of the intermolecular complexes depend on the temperature of the systems. In

the cases of normal pressure and temperature lower than zero degrees centigrade the water molecules are most ordered. It is a crystalline state with hexagonal structure. A unit cell is made up of four water molecules. Four oxygen atoms at the corner of regular tetrahedron surround a central oxygen atom at distance of 2.76 Å. It is less than the sum of van der Waals's radii of oxygen atoms equal to 3.06 Å.

In one hydrogen bond the long bond is about 1.65 Å and the short bond is only 1.11 Å. In the dimer (H$_2$O)$_2$ in Figure 1 the distributions of charge of the valence electrons around the oxygen atom and the hydrogen atoms are changed in the complex [18–22], when compared with that of single water molecule, thus the electron density distribution is also changed around all the atoms of the reacting molecules in such a case. With the help of the hydrogen bond a water dimer (H$_2$O)$_2$ is formed, its bond energy is about 0.2 ev. This energy is roughly equal to a twentieth of the energy of the covalent bond OH. Each water is joined to its neighbors by four hydrogen bonds, the angle between the OH bonds in the molecules approximates to the "tetrahedral" value of 109°. In the free molecules it is approximately equal to 105°. The structure of ice reminds one of the structure of diamond. However, in diamond there are covalent chemical forces which act between the carbon atoms. The diamond crystal is a large molecule. Ice crystals belong to the class of molecular crystals. The molecules in the crystal essentially retain their identity and support each other by hydrogen bonds.

Experimental observations show that ice crystals exhibit considerable electrical conductivity. Along the chains it is about 10^3–10^4 times larger than that in the perpendicular direction, even though electron transfer through the systems is hardly supported [11–24]. Thus we have the reason to think that there is a series of hydrogen-bonded chains in the ice crystal, the motion of the carriers along these chains causes the electric conductivity of the ice, the carriers are not the electrons, but the hydrogen ions or protons in these hydrogen bonds due to the very strong electronegativity of oxygen atoms. Therefore, the ice crystal is a typical hydrogen bonded system. In ice one unusually considers one-dimensional chains, so-called Bernal-Fowler filaments. In a normal state the two kind of arrangements of the type OH‒H....OH‒H....OH‒H....OH‒H and the type H‒OH....H‒OH....H‒OH.....H‒OH have the same energy. Therefore the potential energy of the proton should have the form of a nonlinear double-well with two minima corresponding to its two equilibrium positions as shown in Figure 2. The barrier of the double-well potential has in general the order of the binding energy of the covalent bond H‒O which is approximately 20 times larger than that in a hydrogen bond. Thus the ice crystal is a nonlinear system, the proton transfer in the hydrogen-bonded systems is a nonlinear problem [20–40]. In such a case it is very necessary to know the mechanism and properties of the proton transfer in the system. We infer from Figure 2 that the states and positions of the protons in the double wells are changed, when the system is perturbed by an
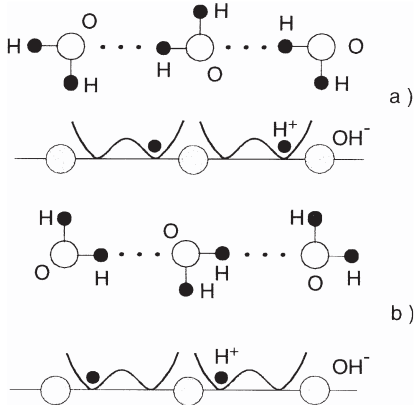
Fig. 2. Potential curve in hydrogen-bonded system of water molecules.

externally applied field. They can migrate to other water molecules from one to form an ionic defect, hydroxonium, H_3O^+, and another water molecule is dissociated by losing one of its protons to its neighbors, forming another ionic defect, hydroxyl, OH^-, each proton (H^+) can be transferred inside the $H\_OH....H$ bridge, interchanging the role of the covalent ($\_$) and hydrogen ($....$) bonds with the oxygen atom. However, when the protons approach the ends of finite chains in the form of ionic defects, they cannot continue through proton transfer, if no re-orientation of OH groups or Bjerrum defects occurs. Therefore, proton transfer can only be carried out by a combination motion of the ionic and bonded defects in the hydrogen-bonded system.

According to the above features of structure of the water molecule and the nonlinear property of the proton transfer in ice, Antonchenke, Davydov and Zolotaryuk (ADZ model) first proposed the nonlinear soliton model of proton transfer in 1980s [20,23]. In this model, an ionic defect appears as a kink or solitary wave in the proton sublattice which propagates together with a localized deformation of the relative distance between neighboring oxygen atoms. Therefore the soliton is only determined by the double-well potential. The coupling interaction between the proton and OH group provides only one mechanism to reduce the height of the barrier of the double-well potential which the protons have to overcome to pass from one molecule to another. Thus this model can only explain the motion of an ionic defect, not the motion of a bonded defect in the system [34–42]. Meanwhile, these models are also very difficult to solve, so that no exact analytical solution can be given. If realistic values for the systems are considered, the continuum approximation fails due to the narrowing of the domains of validity of the solutions with respect to the lattice spacing. This is the case in ice in which the H_3O^+ and OH^-ions become almost point defects [34–44].

We recently proposed a new two-component model [40–44] to study the properties of the proton transfer in the hydrogen-bonded systems. The Hamiltonian in this model includes not only the change of the

relative positions of neighboring oxygen atoms, arising from the motion of the proton, but also the resonant or dipole-dipole interaction between neighboring protons and the change of relative positions of neighboring oxygen atoms, arising from this interaction. In this model the motion of the proton is determined by competition of the double-well potential and the nonlinear coupling interaction between the proton and oxygen atoms. The motion of a proton between a pair of oxygen atoms crossing a double-well potential, which causing ionic defects to occur, is mainly determined by the double-well potential; the coupling interaction only reduces the height of the barrier which the proton has to overcome. However, when the proton approaches the neighboring oxygen atom, the coupling interaction is greatly enhanced and can be so much larger than the double-well potential that the proton can shift over this barrier by this interaction in terms of a quasi-self-trapping mechanism. Thus a bonded defect occurs in such a case. Therefore the above model can explain completely the proton transfer in hydrogen bonded systems. However, this model works only in the classical case. In the following we generalize it to the quantum case to study the mobility and conductivity of the protons in ice for exposing the mechanism of magnetization of water.

The one-dimensional model with two components used in our model and the corresponding double-well potential of the proton represented by $U(r_n) = U_0[1 - (\frac{r_n}{r_0})^2]^2$ are shown in Figure 3. If considering further the elastic interaction caused by the covalent interaction and the coupled interaction between protons and oxygen atoms and the resonant or dipole-dipole interaction between neighboring protons and the changes of relative positions of neighboring oxygen atoms, resulting from this interaction, as well as the harmonic model with acoustic vibrations of low frequency for the oxygen atomic sublattice, then the Hamiltonian of the systems can be expressed by [40–44]

$$H = H_p + H_{\text{ion}} + H_{\text{int}} =$$
$$\sum_n \left[\frac{1}{2m}p_n^2 + \frac{1}{2}m\omega_0^2 r_n^2 - \frac{1}{2}m\omega_1^2 r_n r_{n+1} \right.$$
$$\left. + U_0\left[1 - \left(\frac{r_n}{r_0}\right)^2\right]^2\right] + \sum_n \left[\frac{1}{2M}P_n^2 + \frac{1}{2}\beta(R_n - R_{n-1})^2\right]$$
$$+ \sum_n \left[\chi_1 m(R_{n+1} - R_n)r_n^2 + m\chi_2(R_{n+1} - R_n)r_n r_{n+1}\right]$$
$$\tag{1}$$

where the proton displacements and momentum are r_n and $p_n = m\dot{r}_n$, respectively, the first being the displacement of the hydrogen atom from the middle of the bond between the nth and the $(n+1)$th oxygen atoms in the static case. r_0 is the distance between the central maximum and one of the minima of the double-well, U_0 is the height of the barrier of the double-well potential. Similarly, R_n and $P_n = M\dot{R}_n$ are the displacement of the oxygen atom from its equilibrium position and its conjugate momentum, respectively. $\chi_1 = \partial\omega_0^2/\partial R_n$ and
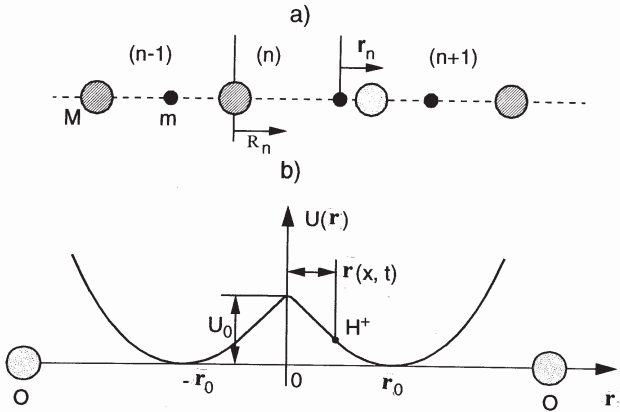
Fig. 3. One-dimensional lattice model of the double-well potential in the hydrogen-bonded systems.

$\chi_2 = \partial\omega_1^2/\partial R_n$ are coupling constants between the protonic and the oxygen atomic sublattice which represent the changes of the energy of vibration of the protons and of the dipole-dipole energy between neighboring protons due to a unit extension of the oxygen atomic lattice, respectively. $1/2m\omega_1^2 r_n r_{n+1}$ shows the correlation interaction between neighboring protons caused by the dipole-dipole interactions. ω_0 and ω_1 are diagonal and non-diagonal elements of the dynamic matrix of the proton, respectively. ω_0 is also the Einstein resonant frequency of the protonic sublattice. β is the elastic constant of the oxygen atomic sublattice. m and M are the masses of the proton and oxygen atom, respectively. $C_0 = R_0 (\beta/M)^{1/2}$ is the velocity of sound in the oxygen atomic sublattice, and R_o is the lattice constant. r_0, R_n and r_n and U_0 are shown in Figure 3. The part H_P of H is the Hamiltonian of the protonic sublattice with an on-site double-well potential $U(r_n)$, H_{ion} being the Hamiltonian of the oxygen atomic sublattice with low-frequency harmonic vibration and H_{int} is the interaction Hamiltonian between the protonic and oxygen atomic sublattices. Therefore, each term in equation (1) has a clear physical meaning. This model is significantly different from the ADZ model [23] and the model of Pnevmatikos et al. [29,34,35], although it is also a coupled model of two oscillators (proton and oxygen atom), due to the following reasons. (1) So far as the state and motion of the oxygen atom in our model is concerned, it is only a harmonic oscillator with low-frequency acoustic-vibration due to its large mass. However, the oxygen atom has both acoustic and optical vibrations in the ADZ model. The physical idea, which is rather vague, we think is that the optical and acoustic vibrations are two different forms of vibration. We regard our model for the oxygen atom to be more appropriate than the ADZ model. (2) As far as the state and motion of the proton lying in the double-well potential is concerned, we here adopted a model of a harmonic oscillator with optical vibration that includes a non-diagonal factor, which comes from the dipole-dipole interaction between neighboring protons. (3) Interaction of the proton with the oxygen atoms is represented via the dependence of vibrational frequencies of the proton on the

displacements of the oxygen atoms. The relations between them can be represented by

$$\omega_o^2(R_n) \approx \omega_o^2 + \frac{\partial\omega_o^2}{\partial R_n}(R_n - R_{n-1}) = \omega_o^2 + \chi_1(R_n - R_{n-1}),$$

$$\omega_1^2(R_n) \approx \omega_1^2 + \chi_2(R_n - R_{n-1}).$$

When inserting them into the above protonic Hamiltonian, and again taking into account the effect of the neighboring oxygen atoms in left- and right-hand sides of the protons, it is natural to obtain equation (1). Therefore the above Hamiltonian has high symmetry and a one-to-one relation to the interactions. However the ADZ's Hamiltonian does not. As a matter of fact, the vibration of the proton is acoustic, which is contrary to the oxygen atoms in the ADZ model. This is not reasonable for the proton model we think, because the vibrational frequency of the proton is quite high relative to the oxygen atom due to its small mass and the strong interaction accepted. Moreover the relation of the interactions between the protonic and interactional Hamiltonians in the ADZ model does not have a one-to-one correspondence, the physical meaning of the interaction Hamiltonian is also very vague or difficult to understand in the ADZ model. It cannot give a strictly analytic solution at all, so we do not know what are the real properties and the law of the transfer in this system in the ADZ model. On the other hand, the above Hamiltonian for our model not only includes the optical vibration of the protons and the resonant or dipole-dipole interaction between neighboring protons, but also takes into account the changes of the relative displacement of the neighboring oxygen atoms, resulting from the vibration of the proton and the dipole-dipole interaction between the neighboring protons. Therefore, it can represent reasonably the dynamic features of the system.

We now study the conductivity of protons in ice using this model. Owing to the fact that the proton motion and vibrations of the oxygen atoms are all quantized, we should use a quantum mechanical technique to study it. Thus making the standard transformation

$$r_n = (2m\omega_0/\hbar)^{-1/2}(a_n + a_n^+),$$
$$p_n = (\hbar m\omega_0/2)^{1/2}(-i)(a_n - a_n^+)\ \ (i = \sqrt{-1}), \quad (2)$$

where $a_n^+(a_n)$ is the creation (annihilation) operator of the proton, then equation (1) becomes

$$H = \sum_n \left\{ \hbar\omega_0 a_n^+ a_n - \left[\frac{\hbar\omega_1^2}{4\omega_0} - \frac{\hbar\chi_2}{2\omega_0}(R_{n+1} - R_n) \right] \right.$$

$$\times (a_{n+1}^+ + a_{n+1})(a_n^+ + a_n) + U_0 \left[1 - \frac{\hbar}{m\omega_0 r_0^2}(a_n^+ + a_n)^2 \right.$$

$$\left. + \frac{\hbar^2}{4m^2\omega_0^2 r_0^4}(a_n^+ + a_n)^4 \right] + \frac{\hbar\chi_1}{4\omega_0}(R_{n+1} - R_{n-1})(a_n^+ + a_n)^2$$

$$\left. + \left[\frac{M}{2}\dot{R}_n^2 + \frac{\beta}{2}(R_{n+1} - R_n)^2 \right] \right\}. \quad (3)$$

The proton motion is a non-linear problem because there is the fourth power of operator a_n(or a_n^+) in equation (3), which is caused by the double-well potential and coupling interaction between the proton and vibrational quantum (phonon) of the oxygen atoms. In such a system, the collective excitations, arising from these nonlinear interactions which result in a localized fluctuation of the protons and the deformation of structure of the oxygen atomic sublattice, have, in general, coherence [33], Therefore we should adopt coherent or quasi-coherent states to express these collective excitations. Thus we choose a wave function for the systems of the form

$$|\Phi\rangle = |\varphi\rangle|\beta\rangle = 1/\lambda'(1 + \sum_n \varphi_n(t)a_n^+)|0\rangle_{pr}$$
$$\times \exp\left\{\sum_n 1/i\hbar[u_n(t)P_n - \pi_n(t)R_n]\right\}|0\rangle_{ph} \quad (4)$$

where $|0\rangle_{pr}$ and $|0\rangle_{ph}$ are the ground states of the proton and the vibrational quantum (phonon) of the heavy ionic sublattice, respectively. The $\varphi_n(t)$, $u_n(t) = \langle.\Phi|R_n|\Phi\rangle$. and $\pi_n(t) = \langle.\Phi|P_n|\Phi\rangle$. are three sets of unknown functions. λ' is a normalization factor. We assume hereafter that $\lambda' = 1$ for the convenience of calculation except when explicitly mentioned.

Obviously, the present wave function of the proton, $|\varphi\rangle = (1 + \sum_n \varphi_n(t)a_n^+)|0\rangle_{pr}$, is not an excitation state of a single particle, but rather a coherent state, or more accurately, a quasi-coherent state. To see this, we can, when $|\varphi_n(t)| \ll 1$, represent $|\varphi\rangle$ by

$$|\varphi\rangle \sim \exp\left[-\frac{1}{2}\sum_n |\varphi_n(t)|^2\right]\exp\left[\sum_n \varphi_n(t)a_n^+\right]|0\rangle_{pr} =$$
$$\exp\left\{\sum_n \left[\varphi_n(t)a_n^+ - \varphi_n^*(t)a_n\right]\right\}|0\rangle_{pr}. \quad (5)$$

The last term in equation (5) is a standard coherent state. More precisely, the above wave function retains only two terms of the expansion of a standard coherent state, which mathematically is justified in the case of small $\varphi_n(t)$ (i.e., $|\varphi_n(t)| \ll 1$), which can be viewed as an effective truncation of a standard coherent state. Therefore we refer to $|\varphi\rangle$ or $\Phi\rangle$ as a quasi-coherent state. We can demonstrate that this state contains only one quantum. Therefore, $|\Phi\rangle$ not only exhibits coherent feature of collective excitations of the protons and phonons caused by the nonlinear interaction generated by the proton-phonon interaction, but can also make the wave function of the states of the system be symmetrical, and $1\varphi\rangle$ can make the numbers of protons maintain conservation in the Hamiltonian equation (3). Meanwhile, the above wave function has also another advantage, i.e., the equations of motion of the soliton can be obtained by the Heisenberg equations of creation and annihilation operators [40–45] from equations (3) $\sim$ (4), i.e., from

$$i\hbar\frac{\partial}{\partial t}\langle\Phi|R_n|\Phi\rangle = i\hbar\dot{u}_n = \langle\Phi|[R_n, H]|\Phi\rangle$$

$$i\hbar\frac{\partial}{\partial t}\langle\Phi|P_n|\Phi\rangle = i\hbar\dot{\pi}_n = \langle\Phi|[P_n, H]|\Phi\rangle \quad (6)$$

we get

$$\dot{u}_n(t) = \pi_n(t)/M \quad (7)$$

$$\dot{\pi}_n(t) = \beta(u_{n+1} + u_{n-1} - 2u_n)$$
$$+ \hbar\chi_1/2\omega_0\left(|\varphi_{n+1}|^2 - |\varphi_{n-1}|^2\right)$$
$$- \hbar\chi_2/2\omega_0\left(\varphi_{n-1}\varphi_n^* - \varphi_n^*\varphi_{n+1}\right.$$
$$\left.+ \varphi_{n-1}^*\varphi_n - \varphi_n\varphi_{n+1}^*\right). \quad (8)$$

Therefore, we have

$$M\ddot{u}_n(t) = \beta(u_{n+1} + u_{n-1} - 2u_n) + \hbar\chi_1/2\omega_0(|\varphi_{n+1}|^2 - |\varphi_{n-1}|^2)$$
$$- \hbar\chi_2/2\omega_0(\varphi_{n-1}^*\varphi_n + \varphi_n^*\varphi_{n-1} - \varphi_n\varphi_{n+1}^* - \varphi_n^*\varphi_{n+1}). \quad (9)$$

From

$$i\hbar\frac{\partial}{\partial t}\langle\Phi|a_n|\Phi\rangle = i\hbar\frac{\partial}{\partial t}\varphi_n(t) = \langle\Phi|[a_n, H]|\Phi\rangle \quad (10)$$

$$i\hbar\frac{\partial}{\partial t}\langle\Phi|a_n^+|\Phi\rangle = i\hbar\dot{\varphi}_n^*(t) = \langle\Phi|[a_n^+, H]|\Phi\rangle \quad (11)$$

we get

$$i\hbar\dot{\varphi}_n = \hbar\omega_0\varphi_n - \frac{\hbar\omega_1}{4\omega_0}\left[(\varphi_{n+1} + \varphi_{n+1}^*) + (\varphi_{n-1} + \varphi_{n-1}^*)\right]$$
$$+ \left[\frac{\hbar\chi_1}{2\omega_0}(u_{n+1} - u_{n-1}) - \frac{2\hbar U_0}{m\omega_0 r_0^2}\right](\varphi_n + \varphi_n^*)$$
$$+ \frac{\hbar\chi_2}{2\omega_0}\left[(u_{n+1} - u_n)(\varphi_{n+1} + \varphi_{n+1}^*)\right.$$
$$\left.+ (u_n - u_{n-1})(\varphi_{n-1} + \varphi_{n-1}^*)\right]$$
$$+ \frac{4\hbar^2 U_0}{m^2 r_0^4\omega_0^2}|\varphi_n|^2(\varphi_n + \varphi_n^*) + \frac{3\hbar^2 U_0}{m^2 r_0^4\omega_0^2}(\varphi_n + \varphi_n^*). \quad (12)$$

$$i\hbar\frac{\partial\varphi_n^*}{\partial t} = -\hbar\omega_0\varphi_n^* + \frac{\hbar\omega_1}{4\omega_0}\left[(\varphi_{n+1}^* + \varphi_{n+1}) + (\varphi_{n-1}^* + \varphi_{n-1})\right]$$
$$- \left[\frac{\hbar\chi_1}{2\omega_0}(u_{n+1} - u_{n-1}) - \frac{2\hbar U_0}{m\omega_0 r_0^2}\right](\varphi_n^* + \varphi_n)$$
$$- \frac{\hbar\chi_{21}}{2\omega_0}\left[(u_{n+1} - u_n)(\varphi_{n+1}^* + \varphi_{n+1})\right.$$
$$\left.+ (u_n - u_{n-1})(\varphi_{n-1}^* + \varphi_{n-1})\right]$$
$$- \frac{4\hbar^2 U_0}{m^2 r_0^4\omega_0^2}|\varphi_n^*|^2(\varphi_n^* + \varphi_n) - \frac{3\hbar^2 U_0}{m^2 r_0^4\omega_0^2}(\varphi_n^* + \varphi_n). \quad (13)$$

Thus, we obtain approximately from equations (12, 13).

$$-\frac{\partial^2\varphi_n}{\partial t^2} \approx \omega_0^2\varphi_n - \frac{\omega_1^2}{2}(\varphi_{n+1} + \varphi_{n-1})$$
$$+ \left[\chi_1(u_{n+1} - u_{n-1}) - \frac{4U_0}{mr_0^2}\right]\varphi_n$$
$$+ \chi_2\left[(u_{n+1} - u_n)\varphi_{n+1} + (u_n - u_{n-1})\varphi_{n-1}\right]$$
$$+ \frac{8\hbar U_0}{m^2 r_0^4\omega_0^2}|\varphi_n|^2\varphi_n + \frac{6\hbar U_0}{m^2 r_0^4\omega_0^2}\varphi_n. \quad (14)$$

We can obtain from equations (9) and (14) in the continuum and long-wave approximations [40–45]

$$\frac{\partial^2 \varphi_n}{\partial t^2} = \varepsilon' \varphi + \frac{\omega_1^2 R_o^2}{2} \frac{\partial^2 \varphi}{\partial t^2} - 2(\chi_1 + \chi_2) R_o \frac{\partial u}{\partial x} \varphi$$
$$- \frac{8\hbar U_o}{m^2 r_o^4 \omega_o} |\varphi|^2 \varphi = f_1(\varphi, u) \quad (15)$$

$$M \frac{\partial^2}{\partial t^2} u(x,t) = \beta R_0^2 \frac{\partial^2}{\partial x^2} u(x,t)$$
$$+ \hbar R_o \frac{(\chi_1 + \chi_2)}{\omega_o} \frac{\partial}{\partial x} |\varphi(x,t)|^2 = f_2(\varphi, u) \quad (16)$$

where $\varepsilon' = \omega_1^2 - \omega_0^2 + \frac{4U_0}{mr_0^2}(1 - \frac{3\hbar}{mr_0^2 \omega_0})$

Assuming $\xi = x - vt$, again from equations (15, 16) we can get:

$$\frac{\partial u}{\partial x} = -\frac{(\chi_1 + \chi_2)\hbar R_0}{MC_0^2(1 - s^2)\omega_0} |\varphi(x,t)|^2 + A \quad (17)$$

$$\frac{\partial^2 \varphi}{\partial t^2} = \varepsilon \varphi + v_1^2 \frac{\partial^2 \varphi}{\partial x^2} - g|\varphi|^2 \varphi \quad (18)$$

where

$$\varepsilon = \varepsilon' - 2A(\chi_1 + \chi_2)R_0,$$
$$g = \frac{8\hbar U_0}{m^2 r_0^4 \omega_0} - \frac{2R_0^2(\chi_1 + \chi_2)^2}{MC_0^2(1 - s^2)\omega_0},$$
$$v_1^2 = \frac{1}{2}\omega_1^2 R_0^2, s = v/c_0. \quad (19)$$

A is an integral constant. From equations (18, 19) we see clearly that there is two equally nonlinear interactions, the double-well potential and coupled interaction between the proton and oxygen atom, in this model. The competition and balance between the two nonlinear interactions results in two kinds of different soliton solutions, which correspond to two kinds of different defects (ionic and bonded defects) in the system. This competition of the two interactions is mainly controlled by the coupled interaction between the protons and heavy ion, $(\chi_1 + \chi_2)$, and proton velocity, v. When the coupling is small, i.e, distance between proton and oxygen atom is large, the effect of the double-well potential is dominant, thus, $g > 0$, $\varepsilon > 0$, the solutions of equations (17, 18) at $0 < v < v_1$, and C_0 are of the form [40–44].

$$\varphi(x,t) = \pm \left(\frac{\varepsilon}{g}\right)^{1/2} \tanh \zeta \left(\zeta = \left(\frac{\varepsilon}{2(v_1^2 - v^2)}\right)^{1/2} (x - vt)\right) \quad (20)$$

$$u(x,t) = \mp \frac{\sqrt{2}(\chi_1 + \chi_2)\hbar R_o}{MC_o^2(1 - s^2)g\omega_o} [\varepsilon(v_1^2 - v^2)]^{1/2} \tanh \zeta \quad (21)$$

$$u(x,t) = B\varphi(x,t), B = \frac{\sqrt{2}(\chi_1 + \chi_2)\hbar R_o}{MC_o^2(1 - s^2)\omega_o} \left[\frac{(v_1^2 - v^2)}{g}\right]^{1/2}. \quad (22)$$

When $g < 0$ and $\varepsilon < 0$, $0 < v_1 < v$, or $v > C_o$, the solutions of equations (17, 18) are still equations (20–22).

Inversely, when the coupling interaction is primary and dominant relative to the double-well potential, then $g < 0$, $\varepsilon < 0$, the solutions of equations (17, 18) are [43,45]

$$\varphi(x,t) =$$
$$\pm \left(\frac{2|\varepsilon|}{|g|}\right)^{1/2} \sec h\zeta' \left(\zeta' = \left(\frac{|\varepsilon|^2}{2(v_1^2 - v^2)}\right)^{1/2} (x - vt)\right) \quad (23)$$

$$u(x,t) = \mp \frac{2(\chi_1 + \chi_2)\hbar R_o}{MC_o^2(1 - s^2)|g|\omega_o} [|\varepsilon|(v_1^2 - v^2)]^{1/2} \tanh \zeta' \quad (24)$$

at $0 < v < v_1, C_o$. When $g > 0$ and $\varepsilon > 0$ and $v_1 < v$, or $C_o < v$, the solutions of equations (17, 18) are still equations (23, 24). Therefore, there are two kinds of different solutions for different parameter values in our model. This shows that the properties of the protons depend mainly on the coupling interactions between the protons and oxygen atoms and the velocity of the proton. Different $(\chi_1 + \chi_2)$ and v can make ε and g different. Thus, the forms and features of soliton solutions change. This shows that the properties of the proton-solitons vary very sensitively with the parameters of the system. We can determine the properties of the solitons, if we know values of the parameters. For ice crystal the accepted values of the parameters are [20–30,37–44] $R_0 = 2.76$ Å, $r_0 = (0.3–0.4)$ Å, $U_0 = 0.22$ eV, $\chi = \frac{\hbar \chi_1}{2\omega_0} = 0.10$ eV/Å, $\chi' = \frac{\hbar \chi_2}{2\omega_0} = 0.011$ eV/Å, $C_0 = 2 \times 10^4$ m/s, $v_1 = (7 - 9.5) \times 10^3$ m/s, $m = m_p$, $M = 17m_p$, $\omega_0 = (1 - 1.5) \times 10^{14}$ m/s, $\omega_1 = (4 - 5) \times 10^{13}$ m/s, thus the amplitude of the soliton in equation (20) is

$$\varphi_m = \left\{ \left[\omega_1^2 - \omega_0^2 + \frac{4U_0}{mr_0^2}\left(1 - \frac{3\hbar}{mr_0^2 \omega_0}\right) - 2A(\chi_1 + \chi_2)R_0\right] \right.$$
$$\left. \times \left[\frac{8\hbar U_0}{m^2 r_0^4 \omega_0} - \frac{2\hbar R_0^2(\chi_1 + \chi_2)^2}{MC_0^2(1 - s^2)\omega_0}\right]^{-1} \right\}^{1/2} \sim 0.941.$$

The width of the soliton or defect is

$$W_k =$$
$$\pi \left(\frac{2(v_1^2 - v^2)}{\omega_1^2 - \omega_0^2 + \frac{4U_0}{mr_0^2}\left(1 - \frac{3\hbar}{mr_0^2 \omega_0}\right) - 2A(\chi_1 + \chi_2)R_0}\right)^{1/2}$$
$$\approx 6.97R_0, \left(\text{here}, A = \frac{\hbar R_0(\chi_1 + \chi_2)}{MC_0^2(1 - s^2)\omega_0} r_o^2\right).$$

(In the above calculation we choose $r_0 = 0.4$ Å, $v_1 = 8.3 \times 10^3$ m/s, $\omega_0 = 1.2 \times 10^{14}$ m/s and $\omega_1 = 4.5 \times 10^{13}$ m/s for the parameters, r_0, v_1, ω_0 and ω_1, respectively.) This result shows that the continuous approximation used in the above calculation is appropriate to this systems [43,45] because the soliton width is larger than the lattice constant R_o, i.e., $W_k \gg R_o$.

In order to determine the behaviors of the solitons, we have to study further the properties of the effective

potential, $U(\varphi)$, of the system corresponding to equations (17, 18) as follows

$$U(\varphi) = \frac{\hbar}{\omega_o}\left[-\varepsilon\frac{1}{2}\varphi^2 + \frac{1}{4}g\varphi^4\right] + U_0. \qquad (25)$$

Obviously, the potential consists of a double-well potential and non-linearly coupled interaction between the proton and oxygen atom. Its nature depends directly on the magnitudes of g and ε. (I), The case of $\varepsilon > 0$ and $g > 0$ implies that the double-well potential plays a main role for determining the properties of the protons, which makes the protons and oxygen atoms become kink-antikink pairs, equations (20, 21), to cross over the barriers in the intrabonds. The coupling interaction between the proton and oxygen atom is only of secondary importance. It reduces only the height of the barrier to make the proton cross easily over the barriers. In such a case the effective potential has two degenerate minima with

$$U_{\min} = -\left(\frac{\varepsilon^2}{4g}\right) + U_0 \text{ at } \bar{\varphi}_0(\xi) = \varphi_{\min}(\xi) = \pm\left(\frac{\varepsilon}{g}\right)^{1/2}. \qquad (26)$$

Therefore $U_{\min}$ and its position, $\bar{\varphi}_0(\xi)$, and the height of the barrier, $\bar{U}_0^*$, of the effective potential depend directly on the magnitudes of g/ε, or put differently, on $(\chi_1 + \chi_2), \omega_0, \omega_1, V$ and U_0. If we let $\chi_1 = \chi_2 = 0$, and $\omega_1 = 0$, then, $U_{\min} \to 0, \bar{\varphi}_0(\xi) = \varphi(r_0)$. In such a case the effective potential, $U(\varphi)$ in equation (25), consists only of the double-well potential, $U(r_n)$, in equation (1), i.e., there is

$$U'(\varphi) = \frac{-2\hbar U_0}{m\omega_o r_0^2}\left(1 - \frac{3\hbar}{2mr_0^2\omega_0}\right)\varphi^2 + \frac{2\hbar^2 U_0}{m^2 r_0^4\omega_0^2}\varphi^4 + U_0 - \hbar\omega_o.$$

Obviously, it is basically the same with $U(r_n)$ in equation (1) with equation (2) except for somewhat different coefficients, due to quantum effect and approximations used in the calculation.

We see from equations (25, 26) that the $\bar{\varphi}_0(\xi)$ increases and $\bar{U}_0^*$ decreases with increasing ε and decreasing g, or in other words, when increasing the coupled constants. Thus the height of the barrier decreases and the positions of the minima of the potential-wells are lengthened relative to the oxygen atoms in such a case. This means that the possibility of transition of protons crossing over the barrier is increased with an increase of the coupling constants. Then, decrease of the height of the barrier, $\Delta U_0 = U_0 - \bar{U}_0^*$, and change of the state at the equilibrium position, $\Delta\bar{\varphi}_0(\xi) = \varphi(r_0) - \bar{\varphi}_0(\xi)$, can be approximately given, respectively, by

$$\Delta U_0 \approx U_0\left[\frac{1}{8} - 1 + (2z - z^2)(y+1) - y\right] > 0 \qquad (27)$$

with

$$\Delta\bar{\varphi}_0(\xi) \approx$$
$$\left(\frac{z}{2}\left(1 + \frac{y}{2}\right) - \frac{y}{2}\right)\varphi(r_0) > 0, \varphi(r_o) = \left[\frac{mr_o^2\omega_o}{8\hbar}\right]^{1/2} \qquad (28)$$

where $z = \frac{8\hbar}{r_0^2\omega_0 m} + \frac{mr_o^2}{U_0}[2A(\chi_1 + \chi_2)R_0 + (\omega_0^2 - \omega_1^2)], 0 < y = \frac{(\chi_1+\chi_2)^2 m^2 r_0^4 R_0^2}{4U_0 MC_0^2(1-s^2)}.$

The equations show that the minima values of the potential change to minus at $\bar{\varphi}(\xi) > \bar{\varphi}_0(\xi)$ from zero at $\bar{\varphi}_0(\xi) = \varphi(r_0)$ in this case, i.e., the larger $(\chi_1 + \chi_2)$, the smaller $\bar{\varphi}_0(\xi)$, the lower the height of the barrier, and the more negative the values of the minima of the potential energy. Thus the possibility for protons jumping over the barriers is greatly enhanced. This shows clearly that the solitons, equations (20, 21), under the case of $\varepsilon > 0$ and $g > 0$ describes the motion of the proton over the barrier of the double-well potential in intrabonds by the mechanism of jumping from one molecule to other. Ionic defects occur in the systems in such a case. These proton-kinks are accompanied by compression or rarefaction of the oxygen atom sublattice around the protonic defects. This soliton with the plus sign in $\varphi(x,t)$ in equation (20) represents a localized reduction in the protonic density (i.e. expansion of the proton sublattice), arising from the motion of a kind of soliton, which amounts to creating a negatively charged carrier and an extended ionic defect moving with a velocity v less than the speed of sound C_0. Therefore the soliton solution corresponds to the OH ionic defect which appeared in the Bernal-Fowler picture. The other soliton solution with minus sign in $\varphi(x, t)$ in equation (20) represents the compression of the protonic sublattice and an increase of the localized proton density which amounts to creating a positively charged carrier and an extended ionic defect. Therefore it corresponds to the H_3O^+ ionic defect. So, the solutions in equations (20, 21) represent the proton transfer in the ionic defects in the intrabonds accompanied by a localized deformation of the oxygen atomic sublattice. Hence we refer to the soliton as a KINK I soliton for convenience.

Also, the $U_{\min}$ and $\bar{\varphi}_0(\xi)$ in equation (26) decrease also with increasing velocity of the proton. This shows that when the velocity of the protons is increased the protons will be far from the original oxygen atoms.

(II) The case of $\varepsilon < 0$ and $g < 0$ corresponding to the soliton solutions, equations (23, 24), means that the coupled interaction between the protons and oxygen atoms plays the main role for determining the properties of the protons. It makes the protons become solitons in order to shift over the barriers in the interbonds by the mechanism of quasi-self-trapping, the double-well potential playing only a minor role. However, the effective potential of the system is still twofold degenerate in such a case and its minima are

$$U'_{\min} =$$
$$\frac{|\varepsilon|^2}{4|g|} - U_0 \approx \frac{MC_0^2(1 - s^2)\omega_0^4}{8R_0^2(\chi_1 + \chi_2)^2}(1 - z')^2(1 + y') - U_0, (A = 0) \qquad (29)$$

at

$$\bar{\varphi}_0'(\xi) = \pm \left(\frac{|\varepsilon|}{|g|}\right)^{1/2} \approx \pm \varphi_0' \left(1 - \frac{1}{2}z'\right)\left(1 + \frac{1}{2}y'\right),$$

$$\left(\varphi_0' = \left(\frac{MC_0^2(1 - s^2)\omega_0^3}{2R_o^2(\chi_1 + \chi_2)^2}\right)^{1/2}\right) \quad (30)$$

$$0 < z' = \left[\frac{4U_0}{mr_0^2\omega_o^2}\left(1 - \frac{3\hbar}{2mr_0^2\omega_0}\right) - \omega_1^2/\omega_0^2\right], \, 0 < y' = \frac{1}{y}.$$

Obviously, from equations (29, 30), we see that when $(\chi_1 + \chi_2)$ and v increase, then $\bar{\varphi}_0'(\xi)$ decreases. This shows that strong coupling interaction and higher velocities of the proton make it approach other oxygen atoms, so that the distance between the proton and oxygen atoms decreases greatly. Conversely, $\bar{\varphi}_0'(\xi)$ increases, when the $(\chi_1 + \chi_2)$ and v decrease. This means that the coupled interaction between them and the velocities of the protons also decrease with increasing distance. Because there are two new equilibrium positions of the proton in such a case, the proton can shift to another side from one of the oxygen atoms by means of the mechanism of quasi-self-trapping and attraction interaction between the proton and the oxygen atom with negative charge. Thus the rotation of the bond, or Bjerrum defect occurs in such a case. Therefore, the soliton solutions, equations (23, 24), in the case of $\varepsilon < 0$ and $g < 0$ represent the motions of the protons across the barriers in the interbonds at the oxygen atoms, i.e., it represents the Bjerrum defects produced by the rotation of the bond X–H, arising from changes of the relative positions of the protons and the oxygen atoms, in which an O–O bond with two protons in the ice and positive effective charge (the D Bjerrum defect) and one without proton and with negative effective charge (the L Bjerrum defect) occur. Hence we may refer to this type of soliton as a KINK II. The plus sign of $\varphi(x, t)$ in equation (23) applies to the L Bjerrum defect, which amounts to creating a negative effective charge, and the minus sign in $\varphi(x, t)$ in equation (24) applies in the case of the D Bjerrum defect which amounts to creating a positive effective charge.

Therefore, our model supports really two types of different defects occurring in the hydrogen bonded systems due to competition of two types of nonlinear interactions, double-well potential and coupled interaction. This may be summarized as KINK I→I ionic defect, KINK II→L Bjerrum defect and anti-KINK I→I$^+$ ionic defect, anti-KINK II→D Bjerrum defect. What distinguishes them is the type of the non-linear interactions and the way the relative positions of the proton and oxygen atoms change in these phenomena. The ionic defect is mainly produced by the double-well potential through the mechanism of jumping over the barriers in the manner of translation and crossover in the intrabonds, but the Bjerrum defect is caused by coupled interaction through the mechanism of quasi-self-trapping in the manner of lattice deformation and relative shift of positions of two bodies in the interbonds. In the transfer process the protons cross over

the barriers in the intrabonds in the form of kink solitons (which result in the ionic defect), and shift over the barriers in the interbonds in another soliton form (which result in the Bjerrum defect). The reason for this change is that the coupling interaction between the proton and oxygen atom changes with altering of the relative positions between them. When the protons cross the barriers in the intrabonds, the coupling interaction is small due to their long distance from the oxygen atoms, thus, it plays a secondary part in determining the properties of the protons. When the protons are near the oxygen atoms and cross over the barriers in the interbonds, the coupling interaction becomes so great that their positions relatively to those of the oxygen atoms change considerably by means of the mechanism of quasi-self-trapping. In such a case the coupling interaction determines the principal properties of the protons, the latter transforming into another soliton form in the interbonds. However, the changes of the forms of proton transfer are not very sudden, but asymptotic. This point can be explained from the changes of the potential of the system with the change of coupling constant, $(\chi_1 + \chi_2)$, in equations (27–30). As a matter of fact, we see from equations (27, 28) that the minima of the potential energy become more and more negative with increasing $(\chi_1 + \chi_2)$. When the coupling interaction become so great that it is greater than the double-well potential, the minima of the potential energy of the system is just equations (29, 30). Certainly, in the above process the changes of velocity of the proton transfer in different regions can also result in some changes of the potential energy of the system; thus it can also influence to some extent the form of the proton transfer as mentioned above. Because the above solitons are related to the dynamics of charged defects, their motion will result in electrical conductivity in these systems, which is studied in the next section.

3 Mobility and conductivity of the proton transfer

We see from equations (20, 21) that if the nonlinearly autolocalized excitation in the protonic sublattice is a kink (or antikink) there is also an antikink (or kink) soliton in the oxygen atom sublattice, which is a "shadow" of the kink (or antikink) as shown in Figure 4. They propagate along the hydrogen-bonded chains in pairs with the same velocity. In Figure 4 the curve 1(3) corresponds to the kink (antikink) soliton in the protonic sublattice and curve 2(4) corresponds to the antikink (kink) soliton in the oxygen atom sublattice. The momentum of the kink-antikink pair can be represented by [40–42]

$$P = \frac{1}{R_0}\int\left(\frac{\hbar}{\omega_0}\varphi_x\varphi_t + MR_xR_t\right)dx = P_K + P_{ak} = M_{sol}v \tag{31}$$

where $M_{s01} = m_k^* + m_{ak}^*$, $m_k^* = \frac{2\sqrt{2}\hbar\varepsilon^{3/2}}{3(v_1^2 - v^2)^{1/2}gR_o\omega_o}$ and $m_{ak}^* = \frac{2\sqrt{2}MB^2\varepsilon^{3/2}}{3(v_1^2 - v^2)^{1/2}gR_o}$ are effective masses of the kink and antikink, respectively, which can be calculated when
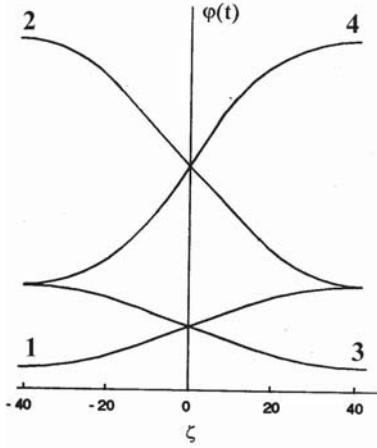
Fig. 4. The kink-antikink soliton pairs in the hydrogen-bonded systems.

equations (20–22) or equations (23, 24) inserting into equation (31), v is velocity of the kink-antikink pair, where $P_K = \frac{1}{R_0} \int (\frac{\hbar}{\omega_0} \varphi_x \varphi_t) dx$, ..and.. $P_{ak} = \frac{1}{R_o} \int (M R_x R_t) dx$ are the momenta of the kink and antikink, respectively. We can find the mobility and conductivity of the proton in the systems using equation (31) because we must know its velocity for finding the conductivity and the momentum of motion of the kink-antikink pair.

We know that the chain is neutral in the absence of any kind of defects in the normal case, but when solitons occur, arising from the displacement of the proton and distortion of the oxygen atom sublattice, the charge deviates from the regular protonic charge distribution in the system. Therefore, the solitons are charged. The charge is related to the quantity $d = R(\infty) - R(-\infty)$, which is equal to $\pm 2R_0$ for positive-negative ionic defects, and $\pm(4\pi - R_0)$ for D and L bonded defects, respectively. Since the proton transfer is caused by a combined transition of the ionic and bonded defects in the systems, thus we can get $q = q_I + q_B$, where q_I and q_B are the charged portions of an ionic and bonded defect, respectively. According to Pnevmatikos et al.'s results [33–35], $q_i = -\alpha_i d_i$ (i is I and B here). When $\alpha_I = \alpha_B = \alpha$, the coefficient of proportionality is found to be $\alpha = q/4\pi$. In most of the systems, $\alpha_I \neq \alpha_B$, and q_i is expected to be strongly dependent on the dynamics of the oxygen atoms.

Utilizing the features of the kink-solitons we can study and calculate the mobility and electrical conductivity caused by motion of the protons or kink-antikink pairs with certain charges from equation (31) in an externally applied electric-field.

Obviously, when an external field is applied to the system, both the protons and oxygen atoms are affected, but the responses in the two sublattices are different, so we should designate the effects to proton and oxygen atom by different fields F_1 and F_2. Then we generalize the above model to include the additional terms in the equations of motion equations (15, 16). When the protons move in the externally applied field we have to consider damping effects to motion in the systems. Thus, the equations of

motion, equations (15, 16), should be replaced, in such a case, by

$$\varphi_{tt} = f_1(\varphi, u) - \Gamma_1 \varphi_t - \left(\frac{m\omega_o}{\hbar}\right)^{1/2} F_1/m,$$

$$u_{tt} = f_2(\varphi, u)/M - \Gamma_2 u_t - F_2/M \quad (32)$$

where F_1 and F_2 are the external forces to the proton and oxygen atom, respectively, and Γ_1 and Γ_2 are the damping coefficients to the motions of the proton and oxygen atom, respectively. Assuming now that the effects of the external force and damping to the kink-antikink pair of equations (20, 21) is so small that they lead only to a small change of the velocity of the kink-antikink pair, but do not alter its waveform, and that the forces, F_1 and F_2, are only functions of time and considering further the boundary conditions of $\varphi(x, t)$ and $u(x, t)$, then we obtain the following equation from equations (31, 32)

$$\frac{dv}{dt} + \gamma v = \left[\frac{3\sqrt{2g}(v_1^2 - v^2)}{2\varepsilon(m + B^2 M m\omega_0/\hbar)} \right] F,$$

$$\gamma = \frac{m\Gamma_1 + B^2 \Gamma M \left(\frac{m\omega_0}{\hbar}\right)}{m + B^2 M \left(\frac{m\omega_0}{\hbar}\right)} + 2v\frac{dv}{dt},$$

$$F = \left(\frac{m\omega_0}{\hbar}\right)^{1/2} F_1 + B \left(\frac{m\omega_0}{\hbar}\right)^{1/2} F_2. \quad (33)$$

Because we assume already that the velocity of the kink-antikink pair is smaller than the sound speeds of the two sublattices, i.e., $v \ll C_o$, $v \ll v_1$, we can neglect the terms including v in the above formulae and regard g, $\bar\varphi_0$, ε, B and γ as constants, i.e., let $g = g_0 =$ const., $B = B_o =$ const., $\bar\varphi_0 = \bar\varphi_0^0 =$ const., $\varepsilon = \varepsilon_o =$ const. $\gamma = \gamma_0 =$ const., then equation (33) becomes

$$\frac{dv}{dt} + \gamma_o v = \frac{3\sqrt{2g_0} v_1}{2\varepsilon_o} \left[m + B_0^2 M \left(\frac{m\omega_0}{\hbar}\right) \right]^{-1} F. \quad (34)$$

Equation (34) is very similar to the equation of motion of a macroscopic particle with damping in classical physics. This shows the classical nature of the kink-antikink pair.

Owing to the fact that the kink-antikink pair has charge, then the electric field force acting on the pair can be represented by $F = q^* E = \left(q_1 + B_0 \left(\frac{m\omega_0}{\hbar}\right)^{1/2} q_2\right) E$ in constant electric field E (where q_1 and q_2 are just the effective charges of the kink and the antikink). Inserting this value into equation (34) we can find the velocity of the kink-antikink pair. It is

$$v(t) = v(0) e^{-\gamma_o t}$$

$$+ \frac{3\sqrt{2g_o} v_1}{2\varepsilon_o} \left[m + B_o^2 M m\omega_o/\hbar \right]^{-1} q^* E (1 - e^{-\gamma_o t}) \quad (35)$$

where $v(0)$ is the initial speed of the kink-antikink pair. When $t \to \infty$, or strictly speaking, the systems are in

steady state after long-time, the velocity of the kink-antikink pair in equation (35) can be denoted by

$$v(t \to \infty) = \frac{3\sqrt{2g_o}v_1}{2\varepsilon_o}\left[m + B_o^2 Mm\omega_o/\hbar\right]^{-1} q^*E. \quad (36)$$

In such a state, a steady current can occur. Thus we can obtain the mobility of the kink-antikink pair in such a case to be

$$\mu = v/E = \frac{3}{\sqrt{2}}\left(q_1 + B_o\left(\frac{m\omega_0}{\hbar}\right)^{1/2}q_2\right)v_1\left(\frac{m\omega_0}{\hbar}g\right)^{1/2} \Big/$$
$$\left[\varepsilon_0\left(m\Gamma_1 + B_0^2\left(\frac{m\omega_0}{\hbar}\right)M\Gamma_2\right)\right]. \quad (37)$$

Thus the electrical conductivity of the kink-antitank pair or proton transfer in the hydrogen bonded systems is

$$\sigma = q^*n_o\mu = \frac{3}{2}\left(q_1 + B_0\left(\frac{m\omega_0}{\hbar}\right)^{1/2}q_2\right)^2 v_1\left(\frac{m\omega_0}{\hbar}g\right)^{1/2} \Big/$$
$$\varepsilon_0\left(m\Gamma_1 + B_0^2\left(\frac{m\omega_0}{\hbar}\right)M\Gamma_2\right) \quad (38)$$

where n_0 is proton numbers in a unit volume. Utilizing preceding actual data and $\Gamma_1 \sim (0.6\text{–}0.7) \times 10^{14}/s$, $\Gamma_2 \sim (9.1\text{–}13) \times 10^{14}/s$, $q_1 = 0.68e$, $q_2 = 0.32e$, $n_0 = 10^{22}$ mol^{-1} for ice [13,20–22,30,41], and using the upper and lower limit values of these parameters we can determine that $\mu = (6.6\text{–}6.9) \times 10^{-6}$m^2/Vs, $\sigma = (7.6\text{–}8.1) \times 10^{-3}(\Omega\cdot\text{m})^{-1}$. The mobility values coincide with Gordon's result [46] obtained by another soliton model which is 7.5×10^{-6}m^2/Vs in ice. These theoretical values of the mobility and electric-conductivity of ice crystals are just in the region of that of semiconductors and are basically consistent with experiment data [17–22,30,39]. Eigen and de Maeyer [39] reported observation of high-mobility proton transfer in ice, which is $(0.05\text{–}0.1)$ cm^2/Vs. Nagle et al.'s experiments [30] found lower protonic mobilities in ice than those initially reported, supporting the belief that earlier reported mobilities might have been the result of surface conduction. Currently reported values are of the order of $(5\text{–}10) \times 10^{-3}$ cm^2/Vs; however, these are still many orders of magnitude larger than mobilities of other ions (such as Li$^+$ and F$^-$) in ice [39]. Obviously, the above value of the mobility, μ, obtained by us is very close to the observed experiment data in the ice crystal. This shows that the above soliton model is appropriate to the ice crystal.

In order to justify further this soliton model of the proton transfer in ice we study further the temperature–dependence of the mobility of the proton by the above soliton model using Nylund et al.'s method [47]. In this way the ice is placed in a heat reservoir and a constant electric-field is turned on for the proton motion. Thus the damping effect and a Langevin-type δ-correlated Gaussian stochastic force are considered in the dynamic equation for the oxygen atom in such a case. In accordance with Nylund et al.'s method we integrate numerically the dynamic equations for the proton and oxygen atom by using the fourth-order Runge-Kutta method. Finally we found the mobility (or velocity) of the thermal kink soliton as a function of inverse temperature for two different field values as shown in Figure 5. In this figure we give also Nylund et al.'s result as a dashed line which was obtained in the same way using the ADZ soliton model. The most distinct feature of the mobility-temperature plots is the presence of two transition temperatures $T_{\max} = 191$ K and $T_{\min} = 210$ K, in other words, when the temperature is increased the mobility rises and a peak occurs around 191 K. Subsequently the mobility drops, reaches a minimum at 210 K, and then rises again. The nonmonotonic up-down-up tendency for this range of temperature seems to be a generic feature in the temperature-dependence of the soliton mobility and can be also observed for other field values and different barrier heights. This behavior is in qualitative agreement with experimental data for the ice crystal in the same temperature range (see the inset in Fig. 5) [11,13], namely, temperature assisted mobility at low and high temperatures with a very distinct drop in the intermediate region occurs in ice. In addition to the qualitative similarity of the conductivity (which was obtained from experiments) and velocity (which is given from the above soliton model) temperature dependences, a most remarkable feature is that the two transition temperatures $T_{\max} = 191$ K and $T_{\min} = 210$ K of the experimental and theoretical data coincide completely. This provides once again one experimental evidence to confirm the existence of the soliton in the ice and shows further that the above soliton model of proton conductivity in the ice crystal are correct and credible.

We should point out here that above model shown in Figure 3, in which all electronic structure calculations of protonated water oligomers are "linear", is only an approximation to a real hydrogen-bonded systems. It is only appropriate to periodic and ideal hydrogen-bonded systems. This is just the limitation of this model. In real ice the influences of spatial structural forms, for example, two- or three-dimensional structures should be also considered. Ste Prevmatikos et al. [32–35] studied the properties of proton transfer in a two-dimensional zig-zag network and demonstrated by one function transformation that there is still soliton motion of the proton transfer in these systems. The features of these solitons resemble the above results. Therefore, the one-dimensional model of the proton transfer in the ice mentioned above is available and as a basic model, it can visually and briefly give the principle features of proton transfer in hydrogen-bonded systems. In order to justify the above theory of proton transfer in ice crystals built by us we here provide two pieces of experimental evidence, i.e., the experimental values of mobility and conductivity and experimental results for the temperature-dependences of mobility coincide completely with our theoretical results. The agreement between the experimental and theoretical results show clearly that the
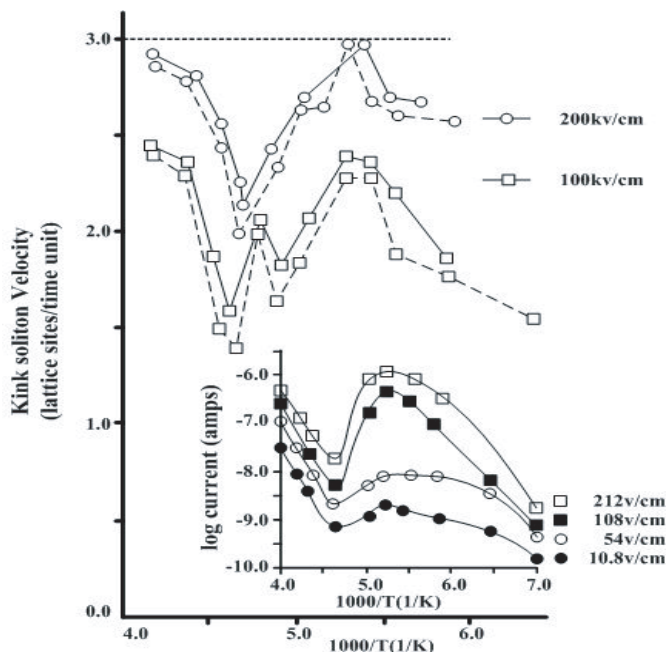
Fig. 5. Kink soliton velocity as a function of inverse temperature for two electric field values, the solid line is our model's result, dashed line is Nylund et al.'s result. The inset in this figure is experimental data [11,13].

above theory of proton transfer in ice crystal built by us is available and correct. These results we obtain here in ice crystals are different from those obtained by ab initio and density functional calculations because the former is a nonlinear excitation theory, but the latter is not so. In the following section we will generalize it to liquid water to study the mechanism and properties of magnetized water.

4 Mechanism, theory and properties for magnetization of water

In this section, we will give the mechanism of the magnetized water and build its theory on the basis of the above theory of proton conductivity in ice crystals and properties of the molecular structure of liquid water.

(1) States and properties of molecules in liquid water

Evidently, states and distribution of molecules in liquid water are different from that in the ice and vapor phases of water, but we cannot forget that ice and vapor can all become water via melting and condensing, respectively. The molecules in liquid water are also polarized [20,48–51], which is easily demonstrated by experiment. If one lets a plastic pen charged with static electricity generated by friction contact the fluid water pouring from a tap, we can clearly see that the fluid water deviates from its original direction and rotates toward the plastic pen. This shows obviously that the molecules in liquid water are polarized. Experiments and calculation show that each water molecule has a dipole-moment of 1.84 Debye. Thus we can believe that there are also a lot of the hydrogen-bonded

chains formed by dipole-dipole interactions between neighboring molecules in the systems which are just like those in ice. Especially at low temperatures, the differences between them are only that the molecular lattice in ice is partially destroyed and the equilibrium positions of molecules are not fixed in water. This is determined by the properties of the first-order phase transition. It is well known that liquid water forms from ice through a first-order phase-transition at the melting point 0 °C. The latent heat is released due to changes of volume and entropy, but its molecular structure has not changed in such a case. Experiments show that the hexagonal structure and hydrogen-bonded chains formed by the hydrogen bonds between neighboring water molecules in the ice can still remain in the liquid water below 4 °C, where the ice lattice is extremely porous and contains many "vacancies" since the number of nearest water molecules to each molecule (coordination number) is only equal to four. On melting the ice lattice is partially destroyed, at the same time some vacancies are filled and the density of water becomes greater than that of ice. This is one of the principal anomalies of water. With further heating up to 4 °C the condensation process continues [20,48–51]. On heating above 4 °C the amplitude of anharmonic vibrations increases, equilibrium positions of these molecules are no longer fixed and the ice lattice is also destroyed, but each molecule has still four neighbors and hydrogen bonds exist still. The contribution of the hydrogen bond to the overall energy of intermolecular interaction (11.6 Kcal/mole) is about 69% in such a state. Because there are a lot of hydrogen bonds, the melting point(0 °C) and boiling point (100 °C) for liquid water are significantly higher than that for other molecular liquids which are only bound together by van der Waals' forces. For example, for methane (CH_4) these values are –186 °C and –161 °C, respectively. Very obviously, the composition and structure of the intermolecular complexes and the number of associated hydro-gen-bonded molecules in the complexes (clusters) and density of water depend on the temperature and decrease with increasing water temperature. This is due to thermally disordered motion of water molecules. Rough estimates give 240 molecules in the clusters at room temperature, 150 at 37 °C and 120 at 45 °C [20]. Therefore, we can confirm that there are always a lot of hydrogen bonded chains in liquid water unless its temperature reaches 100 °C.

Existence of the hydrogen bonds or hydrogen-bonded chains mentioned above can be verified by Raman spectra or infrared absorption spectra of liquid water. Jiang et al.'s [7], Walrafen et al.'s [48–50] and our experiments discovered that there are three peaks in the region of 300–3700 cm^{-1}, 300–900 cm^{-1} and 1600–1900 cm^{-1} and 2900–3800 cm^{-1}, in the Raman spectra of water. Walrafen found further two kinds of translational bands below 300 cm^{-1}. The peak at 300–900 cm^{-1} is associated with the libration of water molecules. The peak at 1600–1900 cm^{-1} is a narrow band, arising from bending vibrations of HOH bonds. The peak at 2900–3800 cm^{-1} is a wide band, containing four peaks, the two peaks at 3281 cm^{-1} and 3416 cm^{-1} correspond to symmetric
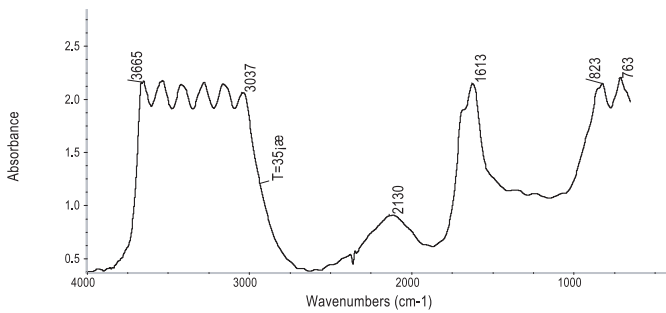
Fig. 6. The infrared absorption spectra of liquid water and the frequency shift of these peaks at 35 °C.

Fig. 7. The hydrogen bonds in the dimer ($\beta = 110°$), the linear hydrogen-bonded. chain ($\beta = 0$) and the circuit hydrogen-bonded chain.

and antisymmetric stretching-vibrations of OH bonds with hydrogen bonds, and the two peaks at 3541 cm^{-1} and 3665 cm^{-1} represent symmetric and antisymmetric stretching-vibrations of OH bonds without hydrogen bonds. Thus we can confirm from these experiments that there are a lot of hydrogen-bonded chains consisting of these hydrogen bonds in the liquid water, in which the hydrogen-bond energy is about 0.2eV. We measured further the infrared absorption spectra of water at 35 °C using the Nicolet Nexus 670-FT-IR spectrometer, which is shown in Figure 6. From this figure we see that there are 6 peaks, 3037, 3165, 3281, 3416, 3541 and 3665 cm^{-1}, in the region of 3000–3700 cm^{-1}, i.e., there are two new peaks at 3037 cm^{-1} and 3165 cm^{-1} in the low frequency range as well as the above four peaks. We confirm again the above conclusion. Thus we can conclude that there are a lot of hydrogen-bonded chains formed by these water molecules except for the free molecules in the liquid water.

Since the Raman and infrared absorption spectra can show the changes in number of the hydro-gen bonds, we can study the nature of the hydrogen bonded chains in liquid water by using the shapes and proportions of the peaks in the 2900–3800 cm^{-1} band. In summary, the above Raman and infrared absorption spectra in the region obtained are consistent with the following interpretation: (1) there are a minimum of four peaks of 3281 cm^{-1}, 3416 cm^{-1}, 3541 cm^{-1} and 3665 cm^{-1} in the region of 2900–3800 cm^{-1} in the Raman and infrared spectra for water which correspond to the symmetric and antisymmetric stretching-vibrations of OH bonds with and without hydrogen bonds, respectively. (2) There are not only free molecules but also a lot of hydrogen-bonded chains consisting of water molecules in liquid water; (3) the numbers of the hydrogen-bonded chains and number of water molecules contained in each chain decrease with increasing water temperature; (4) there is a red-shift of frequencies of these peaks in the Raman and infrared absorption spectra, once the water molecules are incorporated with neighboring molecules by the hydrogen bonds. The more the water molecules are associated, the larger the red-shift.

(2) The closed hydrogen-bonded chain and its features in liquid water

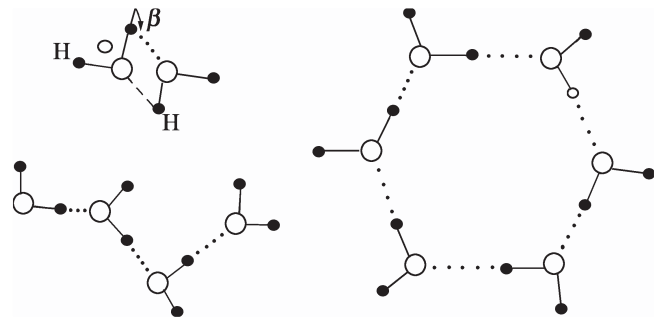From the above result we know that there are a lot of hydrogen-bonded chains, but since linear hydrogen-bonded chains have larger free energy or high energy in liquid water, then they are unstable. Thus, they will necessarily change themselves to lie in stable states with lower energy. If again taking into account the properties for uncertainty of equilibrium positions of the molecules in the liquid water, we can naturally and necessarily confirm that most of the linearly hydrogen-bonded chains can combine mutually and form some closed loop configurations through the linking of head and tail of the linear chains by the hydrogen bonds. Certainly, these closed loop configurations could include the hydrogen-bonded chains containing 2 (dimer), 3, 4, 5, 6 and more water molecules as shown in Figure 7. Obviously, the lower the temperature of the water, then the more the number of water molecules contained in the closed loop. A most evident characteristic of the closed loop formed is that there is an angle between the OH bond and hydrogen bond in this loop. We now represent this angle by β. Clearly, its size depends directly on the number of water molecules or of the hydrogen bonds contained in the closed loops, therefore, it can be used to designate the characteristics of these closed loops. For instance, in the familiar dimer the angle β is 110°, but in the five membered ring it is approximately 30° as shown in Figure 7. Hence, the smaller the angle β, the more the number of water molecules, but this is not a linear relationship. The closed loops formed will result in changes of the frequency shift of the OH stretching-vibrations in them, when compared with the linear hydrogen-bonded chains. In fact, the maximum shift was observed experimentally in the case of the linear hydrogen bond ($\beta = 0$). Experiments and calculations show that for 3281 cm^{-1} the maximum shift is about 260 cm^{-1}, for the 3416 cm^{-1} it is about 320 cm^{-1} [20,52] which is shown in Figure 8. Though the values of the frequency shift depend also on both numbers of water molecules and the angle (β), there is also not a linear relationship between them, in fact this dependent relation is very complicated. We can approximately find this relation according to the above theory of proton transfer in the hydrogen-bonded chains in the ice and the Badger-Bauer rule and the features of the closed loops. We know from the Badger-Bauer rule that the energy of the hydrogen bond is proportional to the shift in frequency, Δv, of the valency
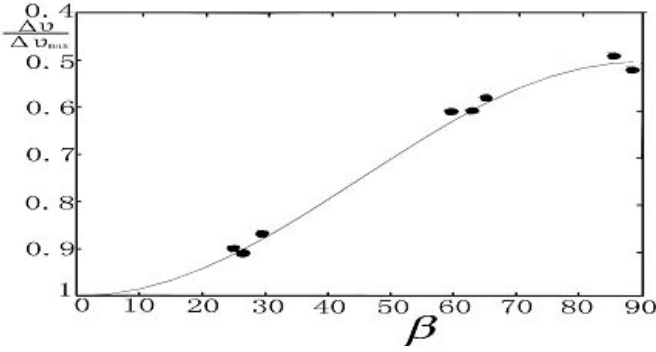
Fig. 8. The ratio of the frequency shift $\Delta v = v_o - v(\beta)$ to the maximum shift $(\Delta v)_{max}$ as a function of the angle β for the ring chains.
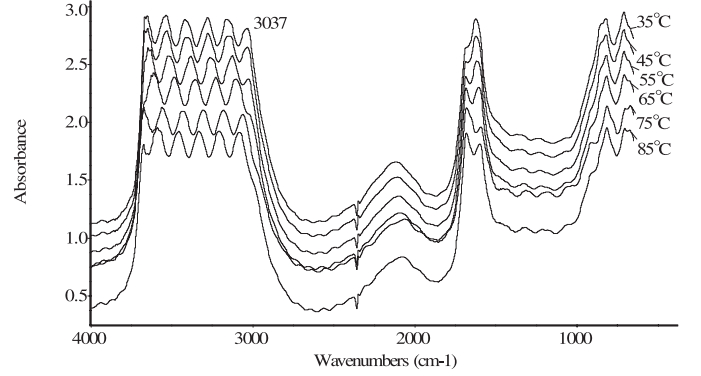

Fig. 9. The infrared absorption spectra of liquid water and the frequency shifts of these peaks at different temperatures obtained by Pang et al.

infrared vibrations of the OH group in the water molecule with respect to the vibrational frequency in the free molecule. From the properties of structure of the closed hydrogen bonded systems, and the interactions and motion model for the proton shown in equation (1) and Figure 3 we approximately found the ratio of the frequency shift $\Delta v = v_0 - v(\beta)$ to the maximum shift $(\Delta v)_{max}$ as a function of the angle β in the closed loops, where $v_0, v(\beta)$ and $v(0)$ are the frequencies of intrinsic vibration and valency infrared vibrations of OH group for $\beta \neq 0$ (closed loop) and $\beta = 0$ (linear chain), respectively, which is shown in Figure 8. The ratio can approximately be represented by

$$\frac{\Delta v}{(\Delta v)_{max}} \sim \frac{v_0 - v_{(0)}\left[1 + \frac{(v_o^2 - v^2(0))}{v_{(0)}^2}(1 - \cos\beta)\right]^{1/2}}{(\Delta v)_{max}}. \tag{39}$$

Therefore, the change of this ratio is plotted by a real curve-line in Figure 8, is approximately consistent with experimental data in real points. This graph also characterizes the dependence of the energy of the hydrogen bond on the angle β. From this figure we not only see that the theoretical result approaches approximately the experimental data [20,52], but also the values of frequency shift decrease with increasing angle β. Alternatively, the frequency, $v(\beta)$, for the closed chain increases when β increases or the number of water molecules contained in the closed chains decreases, but they are not proportional. We can verify experimentally this conclusion by measuring the temperature-dependence of the frequency shift of the infrared absorption of the liquid water. The two new peaks at 3037 cm^{-1} and 3165 cm^{-1} occurring at the sides of low frequency part in Figure 6 should be attributed to the frequency shifts of two peaks of 3416 cm^{-1} and 3541 cm^{-1}, respectively, which is caused by the linear hydrogen-bonded chains becoming closed loops. On the other hand, the size of angle β and numbers of water molecules in the closed loops depend directly on the water temperature, the higher the temperature, the larger the angle β and the smaller the number of water molecules in the closed loops,

thus the larger the values of the frequency shift of the infrared absorption. Therefore, this changed rule of increase of the frequencies of these peaks with increasing of the temperature resembles one of increasing of the frequencies of these peaks with increasing angle β in equation (39) and Figure 8. The former is verified in our experiment. We measured the infrared absorption spectra of water at different temperatures, which is shown in Figure 9. From this figure we see that the frequency of these peaks of water increase, when the temperature of the water is increased. Thus, the rule in equation (39) and above theoretical results obtained for the closed hydrogen-bonded chains are verified by our experiment results shown in Figures 6 and 9. This agreement between theory and experiments make us confirm that not only above idea and theory are correct, but also the closed hydrogen-bonded chains actually exist in the liquid water.

(3) Ring electric-currents in liquid water and the mechanism, theory and properties for magnetization of water

From the above studies we know that closed hydrogen-bonded chains of water molecules are a fundamental feature of liquid water which can be used to account for the magnetization of water. In fact, we knew already from the theory of proton transfer in hydrogen bonded systems described in Section 2 that these closed hydrogen-bonded chains are also the channels for proton transfer, these protons can conduct in the form of proton-solitons with charges along these channels in the liquid water. Thus we can utilize the above theory of proton transfer in ice to study properties of proton transfer in the closed loops and to calculate its mobility and conductivity. Obviously, these rules should be the same as those for ice. The difference between the closed loops and linear chains in the ice is the number of protons participating in the transfers. Hence we can confirm that water can be magnetized due to the fact that these closed loops of the proton conductivity under the action of an externally applied magnetic-field H_{ex} resemble closely the "molecular currents" with magnetism or "small magnets" in solid matter. Concretely speaking, when the liquid water containing a lot of closed hydrogen-bonded chains is exposed in the

H_{ex}, these proton-solitons with velocity v conduct along these closed hydrogen-bond chains, where v is still determined by equation (34), the force, F, in equation (34) is just the Lorenz force, $\vec{F} = q\,\vec{v} \times \vec{H_{ex}}/c$, for these protons which arises from this external-field H_{ex}. Thus the ring electric-current $\vec{J}$ and corresponding magnetic field H_{mol} determined by this $\vec{J}$ occur in these closed loops, they are represented by $\vec{J} = qn\,\vec{v}$ and $\nabla \times \vec{H_{mol}} = 4\pi\,\vec{J}/c$, respectively, according to magnetic theory in physics, where n is the number of the proton-solitons per mole. We here refer to the $\vec{H_{mol}}$ as molecular magnetic field. For a certain closed loop with diameter a, the strength of molecular magnetic field on the symmetrical axis can be represented by $H'_{mol} = 2\pi a^2 J/c(a^2 + Z^2)$ according to the magnetic theory, where Z is the distance of the measurement point on the symmetrical axis with respect to the origin point. Therefore, if only the externally applied magnetic-field and features of the closed loops are known we can find out the sizes of the current J and induced magnetic-field, H_{mol}, by the above formulae and equation (34). Very obviously, there is this molecular magnetic-field for each ring chain, the differences among them are the magnitudes and directions of the molecular magnetic-fields which are due to the distinctions of the conformations of these closed hydrogen-bonded chains, and the numbers of proton and hydrogen-bonds contained in the closed loops. Hence these ring electric-current loops act as "small magnets", and interact each other. However, since the liquid water is always continuously exposed in the externally applied magnetic field, then these "small magnets" will be orderly arrayed along the direction of the externally applied magnetic field in the light of the rule of magnetic interaction. Thus these closed hydrogen-bonded chains also change correspondingly their state and distribution, a locally ordered state of water molecules in these closed loops occurs in the water. Then, the distribution of the water molecules in such a case is different from that in the pure water. Therefore, so-called magnetization of water is just a magnetic-order arrangement of the water molecules in the closed hydrogen-bond chains under the action of the externally applied magnetic-field. Clearly, the stronger the externally applied magnetic-field, the stronger the effect of the magnetic-order orientation, then the stronger the effect of magnetization of the water. Therefore, the magnetization of the water is a paramagnetic effect. Evidently, the changes of the states and distribution of the water molecules as well as the occurrence of the magnetic-order arrangement of the water molecules mentioned above after the magnetization will result necessarily in changes of properties of the water, including the dielectric constant, magnetic coefficient, magneto-conductivity, pH value, Raman and infrared spectra, and so on. Thus, the so-called effect of magnetization of the water is just the changes of properties of water after the magnetization.

From the above mechanism and effect of magnetization of the water we can say that magnetized water has the following properties.
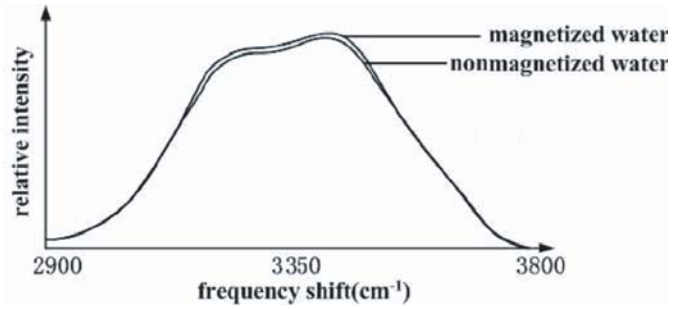

Fig. 10. the Raman spectra of water in the cases of magnetization and without magnetization in the range of 2900–3800 cm^{-1}.

(1) The magnetization of the water is a kind of physical change, instead of chemical change, the structure of the water molecules do not change after the magnetization, the only change is a variation of the states and distribution of water molecules. This can be verified by Raman and infrared absorption spectra of the water which can give insight into the change of structure of the molecules. Pang et al. and Jiang Y.J. et al. and Pang and Dong Ruixin collected [7–10] experimentally the Raman and infrared absorption spectra of a pure and magnetized water using JY-U1000 Raman spectrum Instrument with a power of 400 mw and a source of Ar^+ ionic laser which are shown in Figures 10–12, respectively. From Figures 10–12 we see clearly the strengths of the peaks for the magnetized water are larger than that without magnetized water, but the positions of these peaks do not change, the strengths of the 1500 cm^{-1} peak in the magnetized and pure waters in Figure 11 are 148 and 124, respectively. Therefore, their difference is very obvious. This demonstrates clearly that the structures of water molecules are not varied, the hydrogen bonds are not destroyed.

(2) The magnetized water has a saturation effect and a memory effect. What are the saturation and memory effects of the magnetized water? The so-called saturation effect is just that the properties of magnetized water are not changed, when the externally applied field reaches a certain maximum value; and the memory effect is just that the magnetized effect can still remain some time, when the externally applied field is removed. These properties can be explained easily from the above mechanism and theory of the magnetized water. As a matter of fact, from the above mechanism of magnetized water we know that the magnetized effect depends closely on the size of the proton current $\vec{J} = qn\,\vec{v}$ or the velocity of proton conductivity v. The larger the $\vec{J}$ or v, the larger the molecular magnetic-field $\vec{H_{mol}}$ or H'_{mol}, then the stronger the interaction between the molecular field and externally applied field H_{ex}, thus the stronger the magnetized effect of the water. On the one hand, from equations (34, 35) we know that the velocity v increases proportionally with the externally applied magnetic-field force. However the increase of the velocity is controlled or obstructed by the damping or viscocity effect of the water, so the velocity
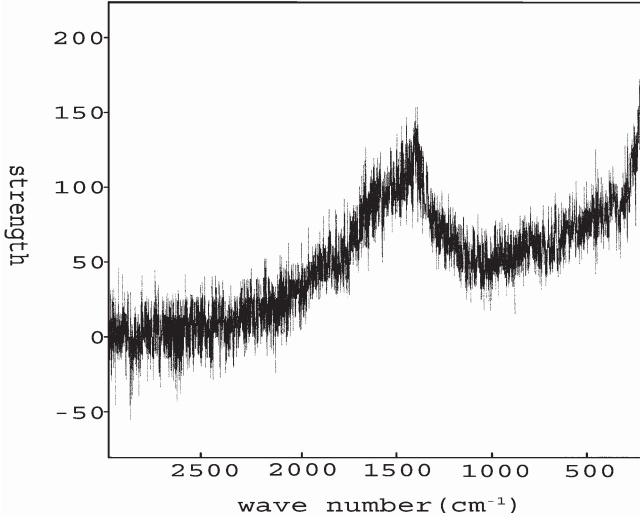
(a)
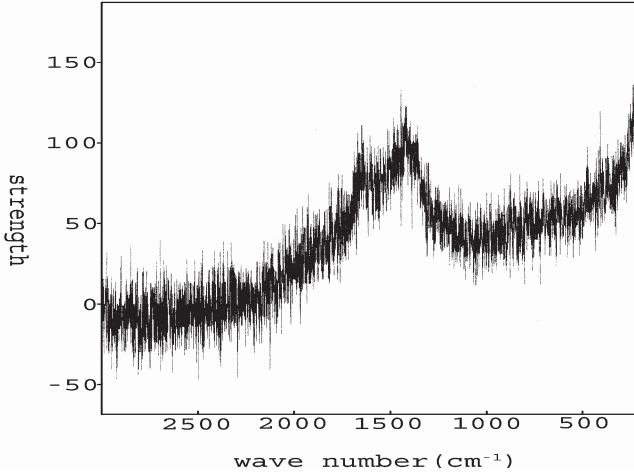
(b)

Fig. 11. the Raman spectra of water with magnetization (a) and without magnetization (b) in the range of 200–2900 cm^{-1} which are obtained by Pang and Dong Ruixin.

Fig. 12. The Infrared absorption spectra of water with magnetization (1) and without magnetization (2) in the range of 200–2900 cm^{-1} obtained by Pang et al.

cannot increase infinitely with increasing of the externally applied field H_{ex}. Thus a maximum value of the velocity and corresponding molecular magnetic-field may occur in certain cases. Hence, there may also be a maximum value for the interactional force between the $\overrightarrow{H_{mol}}$ or H'_{mol} and H_{ex}. On the other hand, the magnetized effect of the water or the magnetic-order arrangement of the water molecules in these closed loops is a result of the interaction between these molecular magnetic-fields and the externally applied field. This magnetized effect is directly related to H_{ex}, the larger the strength of the applied field H_{ex} and the longer the time of magnetization, the larger the magnetized effect, then the stronger the magnetic-order arrangement of the water molecules in these closed loops. When this externally applied field is sufficiently strong, all molecular
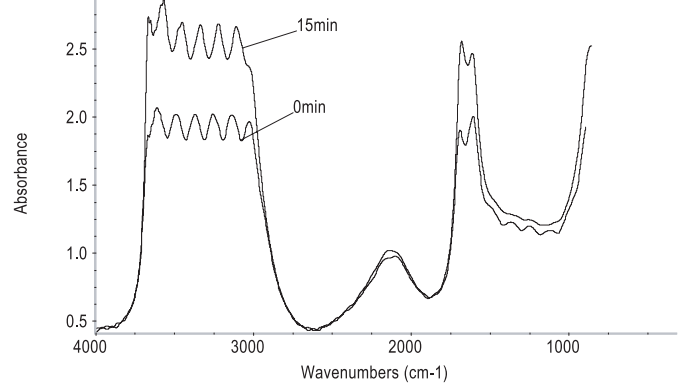
magnetic-fields of the closed loops can be orderly arrayed along the direction of this externally applied field. This is just the saturation phenomenon of magnetization for the liquid water. Obviously, in such a case the saturation magnetic-field can be represented by the linear superposition of the above molecular magnetic fields of all closed loops, it is of the form

$$H_{sa} = \sum_{k=1}^{N} H'_{kmol} = \sum_{k=1}^{N} \frac{2\pi a_k^2 J_k}{c(a_k^2 + Z_k^2)},$$

where N is number of the closed loops in the liquid water, a_k, J_k and Z_k are corresponding values of the kth closed loop, respectively. Evidently, the value of H_{sa} depends on these parameters. In such a case, the total magnetic strength of these closed electric-current loops reaches a maximum, which is represented by the maximum of the absorption peaks in the infrared spectrum. This phenomenon is observed in Pang et al's experiment of infrared absorption of water using a Nicolet Nexus 670-FT-IR spectrometer. In this experiment a glass of 220 ml of pure water is placed on the magnet with magnetic strength of 440 mT. The infrared absorption spectra of the magnetized water at different times are measured. We discover that all peaks maximize suddenly at the moment of 2 h which is shown in Figure 13. This shows that the saturation effect of the magnetized water occurs at this moment. The saturation effect is verified experimentally. This effect was also verified in other experiments [1–10,53–59].

However, this magnetism of the magnetized water does not disappear immediately, when the magnet is suddenly removed from the glass with pure water with saturated magnetization. We observed that it disappeared after about 90 min in our experiment. This denotes that the magnetized water has a memory effect. These phenomena can also be explained by the above theory.

Obviously, this phenomenon is due to the interactions among these molecular magnetic-fields and the damping or viscocity effect of the water. Therefore, the memory effect is just due to the relaxation effect of the magnetized water. In fact, from equation (34) we know that once the externally applied field was removed from the liquid water,
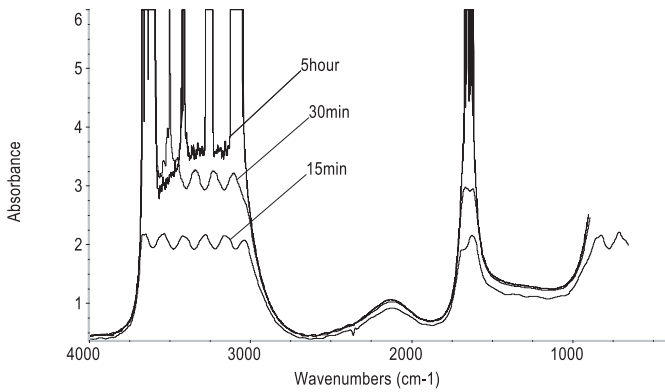
Fig. 13. The saturation effect of magnetization water obtained by Pang et al.

the velocity of motion of the protons in the hydrogen-bonded systems in equation (34) should be represented in the following form

$$\frac{dv}{dt} = -\gamma_o v.$$

Its solution is of the form

$$v(t) = v(0)e^{-\gamma_o t} = v(0)e^{-t/\tau}$$

where $\tau = 1/\gamma_o$ is just the relaxing time of the velocity of motion of the proton in such a case. It shows that the velocity approaches zero, when $t > \tau = 1/\gamma_o$. On the other hand, we know from the above results that the proton electric-current J as well as the molecular magnetic field, H'_{mol}, are proportional to the velocity of motion of the protons, v. This shows that the J and H'_{mol} will also approach zero, when v approaches zero. Thus the interactions among these molecular magnetic-fields eliminate gradually after the time of $\tau = 1/\gamma_o$. Hence, the $\tau = 1/\gamma_o$ is just the lifetime of the proton electric-current J and molecular magnetic-field H'_{in} without the externally applied field. Since this effect exists, then the memory effect of the magnetized water occurs. Evidently, this time is inversely proportional to the damping coefficients, Γ_1 and Γ_2 of the water.

(3) The magnetized effect of water depends on the temperature of the water and decreases with increasing temperature. From the above mechanism of magnetization we know that the magnetic-order arrangement of the water molecules or the magnetization of the water is a result of competition between the magnetic orientation action and thermal disorder effects of the molecules in the water. When the temperature of the water is higher, the kinetic energies of the thermal disorder motions of the water molecules increase. Thus some water molecules could depart from the closed loops. Then the ring electric current decreases on the one hand; the degree of the magnetic-order arrangement of the water molecules for these closed loops is also weakened with increasing temperature due to the increase in thermal damping and relaxation for the water on the other hand. The two effects result in the decrease of the magnetized effect with increasing temperature. This effect is demonstrated by decreases of the

strengths in the infrared absorption with increasing of water temperature which is measured. In our experiment we found that the decrease of the strengths is about 5–8% with each increasing 10 °C. However, we know that the energy of the hydrogen bond is about 0.2eV, the thermal energy of disorder motion of each water molecules, $3KT/2$, is only 0.03–0.05 eV from 20–95 °C. Thus the hydrogen bonds of the water molecules cannot be destroyed by the thermal energy in this region of temperature. Experiments and calculations show that the hydrogen bonds can all be broken at about $T = 100$ °C, in which the water cannot be magnetized. This should be noticed.

(4) The magnetization effect of the water is a nonlinear and locally ordered phenomena and a collective effect for a lot of water molecules, instead of individual behaviors of these molecules.

A direct effect of magnetization of water is to change the states and distribution and density of the molecules in the liquid water. This will result in changes of optics, electrics, mechanics and thermodynamics of water associated with the states and distribution of the water molecules, for example, the dielectric constant, magnetic coefficient, magnetoconductivity, pH value, Raman spectra. A lot of experiments [1–10,53–59] confirm the changes of these physical properties of the liquid water. For example, the dielectric constant, magnetic coefficient, refraction index of light, pH value and magneto-conductivity are increased or enhanced, when the liquid water is magnetized. We measured the change of the refraction index of water after the magnetization at 25 °C by Alber refraction instrument, it becomes 1.3340 from 1.3336. Thus its dielectric constant is also increased. Certainly, these changes are small.

As known, the above model for the magnetization of liquid water is based on the existence of the closed hydrogen-bonded chains on a plane, which is an approximation to real case. In practical liquid water, there is the spatial fluctuations of the hydrogen-bonded network in pico- and sub-pico-second time scale. Very obviously, the fluctuations are caused by disorderly thermal motion of the water molecules and are enhanced with increasing temperature. These fluctuations can influence and go so far as to partially destroy the network structures which will result in decreases of numbers of the circuit hydrogen-bonded chains. However, the energy of the hydrogen bond is larger than the disorderly thermal energy as described above, thus it can completely suppress and restrain the thermal perturbation of the water molecules and the spatial fluctuations of the hydrogen-bonded networks. Hence these closed hydrogen-bond chains cannot be destroyed by these factors, especially in the regions of room and physiological temperatures, except when the temperature of the system approaches 100 °C. However, the destruction effect arising from the spatial fluctuations of the hydrogen-bonded network is a reversible process. When these hydrogen-bonded networks are broken, these networks can also be restored by the fluctuations and uncertainty of positions of water molecules, i.e., the probabilities of destroying and restoring are equal, if the

temperature of the water is maintained. In such a case, even though the numbers of water molecules contained in the hydrogen-bonded networks decreases, these networks cannot be broken, and occur always in the water. Therefore, our point of view is that the thermal perturbation and spatial fluctuations cannot destroy the closed hydrogen-bond chains formed in the water, and can only reduce the number of water molecules contained in these closed loops, especially in the region of room temperature. In such a case the blue shifts of the frequencies of these peaks in the infrared absorption and Raman spectra occur and the magnetized effect of the liquid water are weakened, but are not broken. This idea and knowledge can be verified by Pang et al's experiment shown in Figure 9. From this figure we see clearly that the shapes of the infrared absorption spectra at different temperatures can be kept up to the higher temperature of 85 °C, except for some shifts of the frequency of these peaks. This shows clearly that the closed hydrogen bonded chains formed have been not destroyed completely by the thermal perturbation and spatial fluctuations of water molecules. These arguments and experiments can make us believe that the above theory of magnetization of the water is correct.

In summary, we can use the above theory to explain a lot of phenomena of magnetized water observed in experiment. These results or experimental data strongly support the above mechanism and theory for the magnetization of water.

Finally we should point out that the above idea and theory of magnetization of liquid water are not related to the current states of protons in water proposed by Bingi [60].

5 Conclusions

From the above studies we can obtain the following conclusions for the magnetized water.

(1) We now know that there are a lot of closed hydrogen-bond chains consisting of many water molecules, except for the free water molecules and linear hydrogen-bond chains in liquid water. These closed hydrogen-bond chains act as some "molecular currents" or "small magnets" and are the molecular foundation of magnetization of liquid water. We establish the magnetized theory of liquid water according to the theory of proton conductivity in ice and the properties of pure and magnetized waters. The theory of proton conductivity in ice is confirmed by two experimental results, measurement of the electric conductivity and temperature-dependence of the mobility of the protons. In accordance with rule of the proton transfer in ice crystals we confirm that the conductive carriers of the ring electric-current in the closed loops in the water are the protons, instead of the electrons because the water has formed from the ice through a first order phase transition. The existence of these closed hydrogen-bond chains in the water are verified by our two experiments, measurement of the polarization of water molecules and collection of temperature dependence of the infrared absorption spectra for water, and other experiments [20,52]. Thus, it is credible and reliable. Meanwhile, the results obtained from the

magnetized theory of the water also are completely consistent with the experimental results. Therefore, we can say that the above magnetized theory of water is correct. Notably, according to the above theory and corresponding formulae we could evaluate and determine the distribution of the localized order for the magnetic-arrangements of these water molecules, if we know the numbers of water molecules contained in the closed loops, the numbers and distributions of the closed loops and the strength and direction of the externally applied magnetic-field, H_{ex}. Then we could quantitatively find out the effect of magnetization of water. Evidently, this calculation is very complicated which could be carried out by computer through assuming a model of space-distribution of the closed loops in the liquid water. These problems will be studied in another paper.

(2) Since the mass of the electron is small, so, the velocity of the motion of protons is smaller than that of the electron. Again because the numbers of protons participating in this conduction are less, then the proton current in the closed loops in the water are small. Meanwhile, the water molecules constituting closed hydrogen-bond chains are only a part of the water, thus we can confirm that the magnetized effect of water is very small.

(3) Since the externally applied magnetic-field H_{ex} results only in ring proton-current and molecular magnetic-fields occurring in the closed hydrogen-bonded chains and the magnetic-order arrangement of the water molecules in these closed loops, it neither increases or decreases the number of hydrogen bonds of water molecules in our model, thus, the hydrogen bonds for the water molecules have not been destroyed after the magnetization. Therefore the positions of peaks of Raman scattering and infrared absorption do not change. This is verified by Pang et al.'s and Jiang, et al.'s [7] Infrared absorption and Raman experiments at 35 °C in Figures 10–12. Thus, we can conclude that magnetization can only enhance the strength of the peaks in the infrared absorption and Raman spectra of water, and cannot change their molecular structures. This is just one effect of magnetized water.

(4) Increase of temperature of the liquid water will result in increases of the kinetic energy of disorderly thermal motion of the water molecules and of thermal damping and relaxation for the water, Thus the numbers of water molecule in the closed loops decrease and the degree of the magnetic-order arrangement of the water molecules for these closed loops is also weakened. Therefore, the magnetized effect of liquid water at high temperature is very small relatively to that at low temperature. At $T = 100$ °C, the water cannot be almost magnetized.

(5) The magnetization effect of water is a collective effect for a lot of water molecules, instead of individual behaviors of these molecules. Changes of optics, electrics, mechanics and thermodynamics of water associated with the states and distribution of the water molecules are just a direct effect of magnetized water.

References

1. Xie WenHui, *magnetized water and its application* (Science Press, Beijing, 1983)
2. K.M. Joshi, P.V. Kamat, J. Indian Chem. Soc. **43**, 620 (1965)
3. K. Higashitani, J. Colloid Interface Sci. **152**, 125 (1992); J. Colloid Interface Sci. **156**, 90 (1993)
4. B.N. Ke LaXin, *magnetization of water* (Beijing, Measurement Press, 1982)
5. Zhou Runliang, Zhan Shuxuan, Yuan Liuying, Li Biyu, Chen Shigeng, J. Nature Sin. **8**, 318 (1984)
6. Li Benyuan, Physics Sin. **5**, 240 (1976)
7. Jiang Yijian, Jia Qingjiou, Zhang PengCheng, Xu Lu, J. Light Scattering **4**, 102 (1992)
8. Pan Zhongcheng, Xun Chengxian, J. Chin. Med. Phys. **7**, 226 (1985)
9. Song Dongning, J. App. Math. Mech. **18**, 113 (1997); Cao Changliang, Physics Sin. **22**, 361 (1993)
10. K. Muller, Z. Chem. **10**, 216 (1970); J. Liemeza, Z. Phys. Chem. **99**, 33 (1976)
11. P.V. Hobbs, *Ice Physics* (Oxford, Clarendon Press, 1974); J.J. Derlin, Int. Rev. Phys. Chem. **9**, 29 (1990); L. Onlager, Science **166**, 1359 (1969)
12. R. Podeszwa, V. Buch, Phys. Rev. Lett. **83**, 4570 (1999); V. Buch, P. Sandler, J. Sadlej, J. Phys. Chem. B **102**, 8641 (1998); H. Witek, B. Buch, J. Chem. Phys. **110**, 3168 (1999); S. Kawajima, A. Warshel, J. Phys. Chem. **94**, 460 (1990)
13. H. Engelheart, B. Bullemer, N. Riehl, in *Physics of ice*, edited by N. Riehl B. Bullemer, H. Engelheart (Plemun, New York, 1969)
14. E. Whaley, S.J. Jones, L.W. Grold, *Physics and Chemistry of ice*, Ottawa, RSC, Royal Society of Canada, (1973)
15. H. Bluhm, D.F. Ogletree, C.S. Fadley, Z. Hussian, M. Salmeron, J. Phys.: Condens. Matter **14**, L227 (2002)
16. M.Z. Hubmann, Physica B **32**, 127 and 141 (1974); C. Jaccard, Helv. Phys. Acta, **32**, 89 (1959); K. Koga, H. Tapaka, J. Chem. Phys. **104**, 263 (1996)
17. V.H. Schmidt, J.E. Drumeheller, F.L. Howell, Phys. Rev. B **4**, 4582 (1971); A. Kawada, A.R. McGhie, M.M. Labes, J. Chem. Phys. **52**, 3121 (1970); G. Zundel, *Hydration and Intermolecular Interaction* (Mir. Moscow, 1972), p. 1; *The Hydrogen Bond, Recent Developments in Theory and Experiments*, edited by P. Schuster, G. Zundel, C. Sandorfy (North Holland, Amsterdam, 1976)
18. W.C. Homilton, J.A. Ibers, *Hydrogen bonding in Solids*, (Benjamin, New York, 1969); R.P. Bell, *The proton in chemistry*, (Chapman and Hall, London, 1973); G. Pimentel, A. McClellan, *The hydrogen bond* (Freeman. San Francisco, 1960)
19. M. Eigen, L. de Maeyer, H.C. Spatz, *Physics of ice crystals* (Coll. London, 1962)
20. A.S. Davydov, *Biology and quantum mechanics* (New York, Pergamon, 1982)
21. E. Whalley, S.J. Jones, L.W. Grold, *Physics and chemistry of ice* (Ottawa, RSC, 1973); J.H. Weiner, A. Asker, Nature **226**, 842 (1970); R.J. Nelmes, Ferroelectrics **24**, 237 (1980); H. Granicher, Phys. Kond. Materiel, **1**, (1963)
22. L. Pauling, *The nature of chemical bond* (Cornell University, Ithaca, 1960); T. Bontis, *Proton transfers in hydrogen bonded systems* (Plenum Press, London, 1992)
23. V.Ya. Antonchenko, A.S. Davydov, A.V. Zolotaryuk, Phys. Stat. Sol. (b) **115**, 631 (1983)
24. A.V. Zolotaryuk, R.H. Spatschek, L.E.W. Ladre, Phys. Lett. A **101**, 517 (1984); E.W. Laedke, K.H. Spatschek, M. Wlkens, A.V. Zolotaryuk, Phys. Rev. A **20**, 1161 (1985)
25. A.S. Davydov, *Solitons in molecular systems* (Dordrocht, Kluwer Publisher, 1990), p. 227
26. T. Fraggs, St. Pnevmatikos, E.N. Economon, Phys. Lett. A142, 361 (1989)
27. M. Peyrared, St. Pnevmatikos, N. Flytzanis, Phys. Rev. A **36**, 903(1987); H. Weberpals, R.H. Spatschek, Phys. Rev. A **36**, 2946 (1987); J. Halding, P.S. Lomdahl, Phys. Rev. A **37**, 2608 (1988); R.Mittal, I.A. Howard, Physica D **125**, 179 (1999)
28. D. Hochstrasser, H. Buttner, H. Dosfontaines, M. Peyrared, Phys. Rev. A **38**, 5332 (1988); H. Desfontaines, M. Peyrared, Phys. Lett. A **142**, 128 (1989)
29. St. Pnevmatikos, Phys. Rev. Lett. **60**, 1534 (1988); Phys. Lett. A **112**, 249 (1987); J.M. Braum, Yu. S. Kivshar, Phys. Lett. A **149**, 119 (1990); Phys. Rev. B **43**, 1060 (1991); St. Pnevmatikos, N. Flytzanis, A.R. Bishop, J. Phys. C. Solid State Phys. **20**, 2829 (1987)
30. J.F. Nagle, S.T. Nagle, J. Membr. Biol. **74**, 1 (1983); J.F. Nagle, H.J. Morowitz, Proc. Natl. Acad. Sci. USA **75**, 298 (1976); J.F. Nagle, M. Mille, H.J. Morowitz, J. Chem. Phys. **72**, 3959 (1980)
31. A. Godzik, Chem. Phys. Lett. **171**, 217 (1990)
32. A.V. Zolotaryuk, A.V. Savin, E. Economou, Phys. Rev. B **57**, 234 (1998)
33. A.V. Zolotaryuk, St. Pnevmatikos, Phys. Lett. A **142**, 233 (1996); Yu. S. Kivshar, Phys. Rev; A **43**, 3117 (1991); A.V. Zolotaryuk, M. Peyrared, K.H. Sputschek, Phys. Rev. E **62**, 5706 (2000)
34. St. Pnermatikos, A.V. Savin, A.V. Zolotariuk, Y.S. Kivshar, M.J. Velgakis, Phys. Rev. A **43**, 5518 (1991)
35. St. Pnevmatikos, Y.S. Kivshar, M.J. Valgakis, A.V. Zolotaryuk, Phys. Lett. A **173**, 43 (1993); G.P. Tsironis, St. Pnevmatikos, Phys. Rev. B **39**, 7161 (1989)
36. E.S. Kryachko, Solid Stat. Commun. **65**, 1609 (1988)
37. Y.P. Mei, J.R. Yan, X.H. Yan, J.Q. You, Phys. Rev. B **48**, 575 (1993); Y.P. Mei, J.R. Yan, Phys. Lett. A **180**, 259 (1993)
38. I. Chochliouros, I. Pouget, J. Phys.: Condens. Matter **7**, 8741 (1995); I. Bontis, *Proton transfer in hydrogen bonded systems* (Plenum Press, London, 1992)
39. M. Eigen, L. de Maeyer, Proc. Roy. Soc. A **247**, 505 (1958)
40. X.F Pang (Pang Xiao-feng), H.J.W. Miiller-Kirsten, J. Phys.: Condens. Matter **12**, 885 (2000)
41. X.F. Pang, Y.P. Feng, Chem. Phys. Lett. **373**, 392 (2003); X.F. Pang, G. Zundel, Acta of Phys. Sin. **46**, 625 (1997) and Chinese Physics **7**, 70 (1998)
42. Pang Xiao-feng, A.F. Jalbout, Phys. Lett. A **330**, 245 (2004); X.F. Pang, Chinese Phys. **9**(2), 86 (2000); X.F. Pang, Advance of Physics Sin. **22**, 214 (2002); X.F. Pang, Phys. Stat. Sol. (b) **221**, 1795 (2002)
43. Pang Xiao-feng, *Theory for Non-Linear Quantum Mechanics* (Chinese Chongqing Press, Chongqing, 1994), p. 427 and 795; Soliton Physics (Sichuan Sci. Tech. Press, Chengdu, 2003), pp. 667; Pang Xiao-feng and Feng Yuan-ping, *Quantum mechanics in nonlinear systems*

(World Scientific Publishing Co. New Jersey, 2005), pp. 557–586; Chin. Phys. Lett. **20**, 1662 (2003); X.F. Pang et al., Commun. Theor. Phys. **43**, 367 (2005)

44. X.F. Pang, Phys. Stat. Sol.(b) **236**, 34 (2003); J. Shandong Normal Univ. Sin. (Nature) **15**, 43 (2000); X.L. Yan, R.X. Dong, X.F. Pang, Commun. Theor. Phys. **35**, 615 (2000)

45. X.F. Pang, J. Phys.: Condens. Matter **2**, 9541 (1990); X.F. Pang, Eur. Phys. J. B **10**, 415 (1999) and **12**, 297 (2000); X.F. Pang, Phys. Rev. E **49**, 4747 (1994) and E **62**, 6989 (2000); X.F. Pang, Acta Math. Scienties **13** 437 (1993); X.F. Pang, Chinese Phys. Lett. **10**, 381 and 437 and 517 (1993); X.F. Pang, Chinese Science Bulletin **38**, 1557 and 1665 (1993); X.F. Pang, Acta Physica Slovak **46**, 89 (1998); X.F. Pang, J. Low. Temp. Phys. **58**, 334 (1985)

46. A. Gordon, Physica B **146**, 373 (1987); **150**, 319 (1988); A. Gordon, Solid State Commun. **69**, 1113 (1989)

47. E.S. Nylund, G.P. Tsironis, Phys. Rev. Lett. **66**, 1886 (1991)

48. G.E. Walrafen, J. Chem. Phys. **36**, 1035 (1962); G.E. Walrafen, J. Chem. Phys. **40**, 3249 (1964); G.E. Walrafen, J. Chem. Phys. **44**, 1546 (1966); G.E. Walrafen, J. Chem. Phys. **47**, 114 (1967); G.E. Walrafen, J. Chem. Phys. **48**, 244 (1968); G.E. Walrafen, J. Chem. Phys. **50**, 560 (1969); **52**, 4276 (1970); G.E. Walrafen, M.S. Hokmabadi, W.H. Yang, J. Chem. Phys. **85**, 6964 (1986); G.E. Walrafen, M.R. Fisher, M.S. Hokmabadi, W.H. Yang, J. Chem. Phys. **85**, 6970 (1986)

49. D. Eisenberg, W. Kauzann, *the structure and properties of water* (Oxford, London, 1969)

50. F. Aliotta, M.P. Fontana, Optica Acta, **27**, 931 (1980)

51. S. Myneni, Y. Luo, L.A. Naslund, M. Cavalleri, L. Ojamae, H. Ogasawaea, A. Pelmenschikov, Ph. Wernet, P. Vaterlein, C. Heske, Z. Gussain, L.G.M. Pettersson, A.Nillsson, J. Phys.: Condens. Matter **14**, L213 (2002)

52. A.F. Huxley, Prog. Biophys. Biophys. Chem. **7**, 235 (1957); A.F. Huxley, Nature **173**, 971 (1954)

53. A.D. Koutselose, J. Chem, Phys. **102**, 7216 (1995)

54. M.W. Evans, J. Chem. Phys. **76**, 5473 (1982); M.W. Evans, J. Chem. Phys. **76**, 5480 (1982); M.W. Evans, J. Chem. Phys. **77**, 463 (1982); M.W. Evans, J. Chem. Phys. **78**, 925 (1983); **87**, 6040 (1987)

55. O.G. Mouritsen, Phys. Rev. B **18**, 465 (1978); **22**, 1127 (1980)

56. S. Chikazumi, *Physics in High Magnetic Fields* (Springer-Verlag, Belin, 1981)

57. P.G. Kusalik, J. Chen, Phys. **103**, 10174 (1995)

58. J.C. Dwicki, et al., J. Am. Chem. Soc. **99**, 7403 (1997)

59. K. Binder, *Applications of the Monte Carlo Method* (Springer-Verlag, Berlin, 1984)

60. V.N. Bingi, Biophysics **37**, 502 (1992)